Supersymmetry without *R* parity: Constraints from leptonic phenomenology

Mike Bisset*

Department of Physics, Tsinghua University, Beijing 100084, China
and Department of Physics and Astronomy, University of Rochester, Rochester, New York 14627-0171

Otto C. W. Kong,† Cosmin Macesanu,‡ and Lynne H. Orr§

Department of Physics and Astronomy, University of Rochester, Rochester, New York 14627-0171

R-parity conservation is an *ad hoc* assumption in the most popular version of the supersymmetric standard model. Most studies of models which do allow for *R*-parity violation have been restricted to various limiting scenarios. The single-VEV parametrization used in this paper provides a workable framework to analyze phenomenology of the most general theory of SUSY without *R* parity. We perform a comprehensive study of leptonic phenomenology at the tree level. Experimental constraints on various processes are studied individually and then combined to yield regions of admissible parameter space. In particular, we show that large *R*-parity violating bilinear couplings are not ruled out, especially for large tan β.

I. INTRODUCTION

The minimal supersymmetric standard model (MSSM) incorporates all of the standard model (SM) gauge symmetries in its Lagrangian (see [1,2] for reviews). The MSSM Lagrangian is also constrained by a new discrete symmetry, *R* parity, defined by

$$\mathcal{R} = (-1)^{3B+L+2S} \qquad (1.1)$$

where B, L, and S are respectively baryon number, lepton number, and spin. Imposing *R*-parity conservation prohibits baryon number and lepton number violating terms which could otherwise lead to superparticle-mediated proton decays on a weak interaction time scale, in stark disagreement with observations (for a review and references, see [3]). Because *R*-parity distinguishes ordinary particles from their supersymmetric partners, the minimal model gives rise to a distinctive phenomenology. Supersymmetric particles can be produced only in pairs, and the lightest supersymmetric partner cannot decay. These features drive many, if not most, supersymmetry (SUSY) search strategies.

There is, however, no compelling reason to require *R*-parity conservation. Less restrictive symmetries—conservation of baryon number alone, for example—can be imposed to prohibit unwanted proton decay. Furthermore, *R* parity is not gauged or required by dynamics in the SM or MSSM, and hence there is no theoretical justification for requiring its conservation. It is of course possible to devise extensions of the MSSM in which *R* parity is naturally conserved [4], but such models remain largely *ad hoc*.

Recently there has been a surge of interest in SUSY theories without *R* parity. It is clear that their phenomenology can differ dramatically from that of the MSSM, and must therefore be taken into account in SUSY searches. Introducing *R*-parity violating (RPV) terms into the superpotentials of these theories complicates any analysis enormously. For that reason, most studies make simplifying but otherwise unmotivated assumptions that preclude general application of the results. We have adopted a purely phenomenological approach to supersymmetric theories without *R* parity that provides the framework necessary to greatly simplify analyses without necessitating so many *a priori* assumptions. We introduced our approach in [5] and we elaborate on it here.

The most general renormalizable superpotential without *R* parity for a supersymmetric model with the minimal particle content may be written as

$$
\begin{aligned}
W = \varepsilon_{ab}[& h^u_{ij}\hat{Q}^a_i\hat{H}^b_u\hat{U}^C_j + h^d_{ij}\hat{Q}^a_i\hat{H}^b_d\hat{D}^C_j + h^e_{ij}\hat{L}^a_i\hat{H}^b_d\hat{E}^C_j \\
& + \mu_0\hat{H}^a_d\hat{H}^b_u] + \lambda''_{ijk}\hat{D}^C_i\hat{D}^C_j\hat{U}^C_k \\
& + \varepsilon_{ab}[\lambda'_{ijk}\hat{Q}^a_i\hat{L}^b_j\hat{D}^C_k + \lambda_{ijk}\hat{L}^a_i\hat{L}^b_j\hat{E}^C_k + \mu_k\hat{L}^a_k\hat{H}^b_u],
\end{aligned}
$$
$$(1.2)$$

where i, j, and k are family (flavor) indices. The coefficients λ and λ'' are antisymmetric in the first two indices as required by $SU(2)_L$ and $SU(3)_c$ product rules, respectively. The $SU(2)_L$ indices a and b are shown explicitly contracted with the antisymmetric tensor ϵ_{ab}, with $\epsilon_{12} = -\epsilon_{21} = -1$, to generate $SU(2)_L$ singlets. *R*-parity conservation corresponds to setting $\mu_k = 0$ and all $\lambda = \lambda' = \lambda'' = 0$; for baryon-number conservation, only $\lambda'' = 0$ is required.

We can obtain a more compact form for the superpotential W by noting that the $SU(2)_L$ doublets $\hat{L}_k$ transform under the same SM gauge group representations as $\hat{H}_d$, $[SU(3)_c, SU(2)_L \ U(1)_Y = (\mathbf{1}, \mathbf{2}, \frac{1}{2})]$. (Here the hypercharge Y is normalized such that $Q = T_3 + Y$.) In fact, without the assumption of lepton number conservation, there is nothing to distinguish the $\hat{H}_d$ superfield from the $\hat{L}_k$ superfields, and they can mix. Their separate treatment in Eq. (1.2)

*Email address: bisset@urhepf.rochester.edu

†Email address: kong@pas.rochester.edu

‡Email address: mcos@pas.rochester.edu

§Email address: orr@pas.rochester.edu

is an artifact of starting with the MSSM superpotential and adding R-parity violating terms. Therefore a more appropriate form for W, with extended flavor indices α and β running from 0 to 3, is

$$W = \varepsilon_{ab}[h^u_{ij}\hat{Q}^a_i\hat{H}^b_u\hat{U}^C_j + \lambda'_{i\alpha j}\hat{Q}^a_i\hat{L}^b_\alpha\hat{D}^C_j + \lambda_{\alpha\beta j}\hat{L}^a_\alpha\hat{L}^b_\beta\hat{E}^C_j$$
$$+ \mu_\alpha\hat{L}^a_\alpha\hat{H}^b_u] + \lambda''_{ijk}\hat{D}^C_i\hat{D}^C_j\hat{U}^C_k. \qquad (1.3)$$

$U(4)$ flavor rotations can be used to transform between bases of the four superfield doublets.

It is in principle possible for the neutral scalar component in *each* of these doublets to acquire a non-zero vacuum expectation value (VEV). The key to our approach, the single-VEV parametrization [5,6], is to rotate the doublets into a basis in which $\hat{L}_0$ alone bears a non-zero VEV. The remaining admissible leptonic flavor rotations are sufficient to diagonalize the lepton Yukawas $h^e_{ik} = 2\lambda_{i0k} = -2\lambda_{0ik}$ which are then given by $(\sqrt{2}/v_0)\text{diag}\{m_1, m_2, m_3\}$. There is then no additional freedom to set the μ_k bilinear coefficients equal to zero; to maintain complete generality they must be left arbitrary.

As implied above and discussed in [5,7], care must be taken to specify what choice of flavor basis (if any) is implied when a specific set of of RPV parameters is given. For example, if the sneutrino VEV's and μ_k bilinear terms are left arbitrary, then they are not truly physically independent because of the freedom to rotate between bases. In another extreme, setting all sneutrino VEV's and μ_k bilinears to zero results in a loss of generality, while still not being sufficient to uniquely determine the flavor basis. The common approach of using R-parity conserving MSSM particle states with the *ad hoc* addition of a few RPV trilinear couplings results in ill-defined RPV parameters (since such parameters are in general basis-dependent and the flavor basis is not specified). In principle, that renders the analysis internally inconsistent. In practice, this approach can reasonably approximate some regions of parameter space, but an inherent ambiguity remains. One way out of this quandary would be to construct ''basis-independent'' observables. This has been explored with strong *a priori* restrictions placed on the sneutrino VEV's [8]. However, the observables were found to be phenomenologically ''messy'' and impractical for most experimental situations even in this limiting case. The alternative resolution is to carefully choose a convenient basis that renders the experimental analysis as simple as possible —the path taken in this work with the single-VEV parametrization.

As we described in [5], this parametrization has the advantage that the tree-level mass matrices of *all* fermions in the theory are independent of all trilinear RPV couplings. In particular, R-parity-violating contributions to leptonic phenomenology at tree level are almost entirely determined by the μ_k. In this paper, we examine this tree-level leptonic phenomenology in detail within the single VEV parametrization, focusing on the constraints that can be obtained from existing experimental results. The rich variety of relevant data include precision measurements at the Z^0 pole, charged lepton and pion decay rates and branching ratios, neutrino mass bounds, lepton-neutrino scattering cross sections, and limits on neutrinoless double beta decay. A complete list of the measurements we will use can be found in Table I.

In the present analysis, we assume that these processes are mediated by gauge bosons, i.e., on-shell or off-shell Z^0's or $W^\pm$'s. Scalar intermediaries are also possible for various processes, and these would reintroduce dependence on the trilinear RPV couplings (and other RPV parameters from the scalar sector) even at the tree level. We assume that contributions from such scalar modes are negligible due to kinematic suppression from the presumably much heavier (relative to the gauge bosons) scalars. It is certainly possible in principle that relative strengths of the couplings involved and not-quite-so-heavy scalars may conspire to invalidate our assumption. However, for these to affect our experimental bounds (or for that matter, to be larger than the loop corrections we omit), one has to invoke very special and/or unlikely combinations of parameters. Including the additional parameters needed to accommodate these tiny corners of parameter space needlessly complicates the analysis and will be avoided here. In what follows we will point out neglected scalar modes where appropriate.

We begin our analysis in Sec. II, where we examine the neutral current interactions of the charged fermions (charged leptons and charginos); in Sec. III we do the same for the neutral fermions. We then consider charged current interactions in Sec. IV. Having considered the constraints separately, we then combine them in Sec. V, where we determine exclusion regions in the parameter space from both charged and neutral current processes. Finally, we present a summary of our results and our conclusions in Sec. VI.

II. COLOR-SINGLET CHARGED FERMIONS

The color-singlet charged fermions, the charged leptons and the charginos, are linear combinations of two-component Weyl spinor charged winos (written as $\lambda_\pm$), the spinors of the $\hat{E}_i$ superfields, and the spinors for the charged superfields of the $\hat{L}_\alpha$ and $\hat{H}_u$ $SU(2)_L$ superdoublets. In terms of Dirac spinors for a theory with spontaneous symmetry breaking, denoting spinors corresponding to the superfields in Eq. (1.3) by the corresponding lower-case letters (and where $\tilde{\lambda}$ is the wino and $\tilde{\psi}$ is the ''Higgsino'' built from l_0 and $\tilde{h}_u$), the contributing Lagrangian mass terms are given by

$$\mathcal{L} \ni -(i\bar{\tilde{\lambda}}\,\bar{\tilde{\psi}}\,\bar{l}_1\,\bar{l}_2\,\bar{l}_3)[\mathcal{M}^T_{\mathcal{C}}P_L + \mathcal{M}_{\mathcal{C}}P_R](-i\tilde{\lambda}\,\tilde{\psi}\,l_1\,l_2\,l_3)^T, \qquad (2.1)$$

with
$$\mathcal{M}_{\mathcal{C}} = \begin{pmatrix} M_2 & \dfrac{gv_u}{\sqrt{2}} & 0 & 0 & 0 \\[2mm] \dfrac{gv_d}{\sqrt{2}} & \mu_0 & 0 & 0 & 0 \\[2mm] 0 & \mu_1 & m_1 & 0 & 0 \\[2mm] 0 & \mu_2 & 0 & m_2 & 0 \\[2mm] 0 & \mu_3 & 0 & 0 & m_3 \end{pmatrix}. \qquad (2.2)$$

TABLE I. Summary of phenomenological constraints incorporated in the overall parameter constraint plots. The invisible Z^0 width is assumed to include decays to end states composed of neutrinos and the lightest neutralino. Bounds imposed on Z^0 decay constraints involving charginos and neutralinos are quite conservative, representing uncertainty in signal detection.

Quantity	μ_i combo. constrained	Experimental bounds [9]
	Z⁰-coupling:	
$U_{br}^{e\mu}$ (e-μ universality)	$\mu_1^2 - \mu_2^2$	$(0.596 \pm 4.37) \times 10^{-3}$
$U_{br}^{e\tau}$ (e-τ universality)	$\mu_1^2 - \mu_3^2$	$(0.955 \pm 4.98) \times 10^{-3}$
$U_{br}^{\mu\tau}$ (μ-τ universality)	$\mu_2^2 - \mu_3^2$	$(1.55 \pm 5.60) \times 10^{-3}$
$\Delta\mathcal{A}_{e\mu}$ (e-μ L-R asymmetry)	$\mu_1^2 - \mu_2^2$	$(0.346 \pm 2.54) \times 10^{-2}$ (from $U_{br}^{e\mu}$)
$\Delta\mathcal{A}_{\tau e}$ (τ-e L-R asymmetry)	$\mu_3^2 - \mu_1^2$ + Rt. contrib.	0.0043 ± 0.104
$\Delta\mathcal{A}_{\tau\mu}$ (τ-μ L-R asymmetry)	$\mu_3^2 - \mu_2^2$ + Rt. contrib.	0.082 ± 0.25
$Br(Z^0 \to e^\pm \mu^\mp)$	$|\mu_1\mu_2|$	$<1.7 \times 10^{-6}$
$Br(Z^0 \to e^\pm \tau^\mp)$	$|\mu_1\mu_3|$	$<9.8 \times 10^{-6}$
$Br(Z^0 \to \mu^\pm \tau^\mp)$	$|\mu_2\mu_3|$	$<1.2 \times 10^{-5}$
$Br(\mu^- \to e^- e^+ e^-)$	$|\mu_1\mu_2|$	$<1.0 \times 10^{-12}$
$Br(\tau^- \to e^- e^+ e^-)$	$|\mu_1\mu_3|$	$<2.9 \times 10^{-6}$
$Br(\tau^- \to \mu^- e^+ e^-)$	$|\mu_2\mu_3|$	$<1.7 \times 10^{-6}$
$Br(\tau^- \to \mu^+ e^- e^-)$	$|\mu_1^2\mu_2\mu_3|$	$<1.5 \times 10^{-6}$
$Br(\tau^- \to e^- \mu^+ \mu^-)$	$|\mu_1\mu_3|$	$<1.8 \times 10^{-6}$
$Br(\tau^- \to e^+ \mu^- \mu^-)$	$|\mu_1\mu_2^2\mu_3|$	$<1.5 \times 10^{-6}$
$Br(\tau^- \to \mu^- \mu^+ \mu^-)$	$|\mu_2\mu_3|$	$<1.9 \times 10^{-6}$
$Br(Z^0 \to \chi^\pm l^\mp)$	μ_5	$<1.0 \times 10^{-5}$
$Br(Z^0 \to \chi^+ \chi^\mp)$	μ_5	$<1.0 \times 10^{-5}$
$Br(Z^0 \to \chi_i^0 \chi_j^0, \chi_j^0 \nu); j \neq 1$	μ_5	$<1.0 \times 10^{-5}$
Γ_Z (total Z^0-width)	μ_5	2.4948 ± 0.0075 GeV
$\Gamma_{Z_{inv}}$ (invisible Z^0 width: $Z^0 \to \nu_c \nu_d, \nu_c \chi_1^0, \chi_1^0 \chi_1^0$)	μ_5	500.1 ± 5.4 MeV
	W±-coupling:	
$\bar{\Gamma}^{\mu e}$ ($\mu \to e\nu\nu$)	m_{ν_5}/μ_i ratio	0.983 ± 0.111
$\bar{\Gamma}^{\tau e}$ ($\tau \to e\nu\nu$)	m_{ν_5}/μ_i ratio	0.979 ± 0.111
$\bar{\Gamma}^{\tau\mu}$ ($\tau \to \mu\nu\nu$)	m_{ν_5}/μ_i ratio	0.954 ± 0.108
$R_{\pi\mu}^{\pi e}$ (π decays)	$m_{\nu_5} \Big/ \dfrac{\mu_1}{\mu_5}$ and $\dfrac{\mu_2}{\mu_5}$	$(1.230 \pm 0.012) \times 10^{-4}$
$R_{\tau\mu}^{\tau e}$ (τ decays)	m_{ν_5}/μ_i ratio	1.0265 ± 0.0222
$R_{\tau e}^{\mu e}$ (decays to e's)	m_{ν_5}/μ_i ratio	1.0038 ± 0.0219
$m_{\nu_5}|\bar{B}_{e\nu_5}^L|^2 \, [(\beta\beta)_{0\nu}]$	$m_{\nu_5} \Big/ \dfrac{\mu_1}{\mu_5}$	<0.46 eV (only for $m_{\nu_5} < 10$ MeV)
	mass constraints:	
ν_5 mass	μ_3	<18.2 MeV if $\nu_5 = \nu_\tau$
	μ_5	<149 MeV if $\nu_5 \neq \nu_\tau$
$\chi^\pm$ mass	μ_5	>70 GeV

Here the two vacuum expectation values are in general complex, as are the μ_α's and the soft gaugino mass M_2. As is customary, all of the parameters entering the fermion mass matrices will henceforth be assumed to be real. Potentially very interesting *CP*-violating effects related to the possible complex nature of these parameters will be relegated to a future paper. On the other hand, it must be strongly emphasized that there is no loss of generality concerning the trilinear RPV terms — *these need not be set to zero*. They simply do not appear at the tree level in the fermionic mass matrices in the single-VEV parametrization.

We now wish to find the mass eigenstates. In the MSSM,

the Yukawa mass entries, m_1, m_2, and m_3 ($m_i = h_{ii}^e v_d$ in the single-VEV basis), are identical to the known physical charged lepton masses. Without R-parity conservation this correspondence is spoiled by the presence of the μ_i in $\mathcal{M}_C$. Masses of the well-known charged leptons (and in fact the eigenvectors and mass eigenvalues for all five physical states) now result from diagonalizing the 5×5 chiral mass matrix $\mathcal{M}_C$:

$$U_L^\dagger \mathcal{M}_C U_R = \text{diag}\{\bar{M}_{c1}, \bar{M}_{c2}, \bar{m}_1, \bar{m}_2, \bar{m}_3\}, \qquad (2.3)$$

where U_L and U_R are unitary matrices which diagonalize $\mathcal{M}_C$, and $m_e = \bar{m}_1$, $m_\mu = \bar{m}_2$, and $m_\tau = \bar{m}_3$. In general, the $\bar{m}_i$ depend on the m_i *and* the μ_i.

Therefore for non-zero μ_i the input Yukawa parameters for $\mathcal{M}_C$ need to be determined, i.e. for a fixed set of μ_i, we need to find the values of m_i that give the correct physical masses $\bar{m}_i$. This is done by writing a system of linear differential equations for the infinitesimal change in the m_i's due to an infinitesimal change in the μ_i's. Beginning with all $\mu_i = 0$ (where the solution of the system of equations is known), an acceptable solution for a chosen set of μ_i's is then obtainable via numerical integration [10]. Note that only the three ''lepton'' masses need to be fixed in this way. The heavier so-called ''chargino'' masses $\bar{M}_{c1}$ and $\bar{M}_{c2}$ also depend on the μ_i, but we do not (yet) have experimental constraints telling us what the physical chargino masses should be.

We now consider interactions with the Z^0 boson, following Ref. [11] but using the single-VEV parametrization. The couplings of the five mass eigenstates to the Z^0 boson are given by

$$\mathcal{L}_{\chi^+ \chi^- Z^0} = \frac{g_2}{2 \cos \theta_w} \chi_a^+ \gamma_\mu (P_L \tilde{A}_{ab}^L + P_R \tilde{A}_{ab}^R) \chi_b^- Z^\mu, \tag{2.4}$$

where $\bar{\chi}_a^+ = \chi_a^- = (\chi_1, \chi_2, l_e, l_\mu, l_\tau)$, $P_{R,L} = \frac{1}{2}(1 \pm \gamma_5)$, and

$$\tilde{A}_{ab}^L = U_L^{1a} U_L^{1b} + \delta_{ab}(1 - 2 \sin^2 \theta_w)$$
$$\equiv \delta \tilde{A}_{ab}^L + \delta_{ab}(1 - 2 \sin^2 \theta_w), \tag{2.5}$$

$$\tilde{A}_{ab}^R = 2 U_R^{1a} U_R^{1b} + U_R^{2a} U_R^{2b} + 2 \delta_{ab} \sin^2 \theta_w$$
$$\equiv \delta \tilde{A}_{ab}^R + 2 \delta_{ab} \sin^2 \theta_w \tag{2.6}$$

(notation here follows that of [11] except for the ordering of basis vectors). The δ_{ab} terms are the SM expressions, and deviations from SM expectations originate from non-zero $\delta \tilde{A}_{ab}^L$ and $\delta \tilde{A}_{ab}^R$. The anomalous coupling of any two charged fermions to the Z^0 can thus be determined in terms of the U_L and U_R matrices found numerically from diagonalizing $\mathcal{M}_C$, and this is precisely what we do to obtain the parameter space plots presented later in this paper. The exact analytic expressions for the eigenvalues and eigenvectors of the 5×5 $\mathcal{M}_C$ prove cumbersome and not very illuminating and we do not reproduce them here. However, to improve

our understanding of the results of the exact numerical analysis, it is very useful to consider a couple of interesting analytic approximations.

First, we treat the R-parity violation as a perturbation, taking the limit in which the μ_i are small. If the μ_i were zero, the (now MSSM) chargino sector, which is the upper 2×2 portion of $\mathcal{M}_C$, would be orthogonal to the already diagonal SM charged lepton sector. So first we introduce new 2×2 rotation matrices $R_L(\theta_L)$ and $R_R(\theta_R)$ such that

$$R_L^\dagger \begin{pmatrix} M_2 & \frac{1}{\sqrt{2}} g v_u \\ \frac{1}{\sqrt{2}} g v_d & \mu_0 \end{pmatrix} R_R = \text{diag}\{M_{c1}, M_{c2}\}. \quad (2.7)$$

M_{c1} and M_{c2} are the chargino masses in the $\mu_i = 0$ MSSM limit. Applying this rotation to $\mathcal{M}_C$ we find

$$\mathcal{M}_C' \equiv R_L^\dagger \mathcal{M}_C R_R$$
$$= \begin{pmatrix} M_{c1} & 0 & 0 & 0 & 0 \\ 0 & M_{c2} & 0 & 0 & 0 \\ \mu_1 \sin \theta_R & \mu_1 \cos \theta_R & m_1 & 0 & 0 \\ \mu_2 \sin \theta_R & \mu_2 \cos \theta_R & 0 & m_2 & 0 \\ \mu_3 \sin \theta_R & \mu_3 \cos \theta_R & 0 & 0 & m_3 \end{pmatrix}.$$

$$\tag{2.8}$$

To obtain the general 5×5 U_L and U_R matrices from the MSSM's 2×2 R_L and R_R matrices, we treat the 3×2 off-diagonal block containing the μ_i's as a perturbation. Then

$$U_{L,R}^\dagger = \begin{pmatrix} R_{L,R}^\dagger & -R_{L,R}^\dagger V_{L,R}^\dagger \\ V_{L,R} & I_{3 \times 3} \end{pmatrix}, \tag{2.9}$$

where the elements of the 3×2 V_L and V_R matrices are given by

$$V_L^{i1} = \sqrt{2} \frac{\mu_i M_W \cos \beta}{M_0^2}$$

$$V_R^{i1} = \sqrt{2} \frac{m_i}{M_0} \frac{\mu_i M_W (M_2 \sin \beta + \mu_0 \cos \beta)}{M_0^3}$$

$$V_L^{i2} = -\frac{\mu_i M_2}{M_0^2}$$

$$V_R^{i2} = -\frac{m_i}{M_0} \frac{\mu_i (M_2^2 + 2 M_W^2 \cos^2 \beta)}{M_0^3}, \tag{2.10}$$

and where

$$M_0^2 \equiv \mu_0 M_2 - M_W^2 \sin 2\beta \tag{2.11}$$

which is in fact the determinant of the 2×2 MSSM section of $\mathcal{M}_C$. In the limit of large $\tan \beta$ and/or $\mu_0 M_2 \gg M_W^2$, M_0^2 tends toward $\mu_0 M_2$.

In terms of the V_L and V_R matrix elements, we can now write the deviations of the fermions' coupling coefficients to the Z^0 boson from the SM case as

$$\delta \widetilde{A}_{ab}^L = V_L^{i1} V_L^{j1} = 2 \frac{\mu_i \mu_j}{M_0^2} \frac{M_W^2 \cos^2 \beta}{M_0^2} \qquad (2.12)$$

and

$$\delta \widetilde{A}_{ab}^R = 2 V_R^{i1} V_R^{j1} + V_R^{i2} V_R^{j2} = \frac{m_i m_j}{M_0^2} \frac{\mu_i \mu_j}{M_0^2} \frac{1}{M_0^4} [M_2^4 + 4 M_W^2 \\ \times (M_2^2 + \mu_0 M_2 \sin 2\beta + \mu_0^2 \cos^2 \beta + M_W^2 \cos^4 \beta)], \qquad (2.13)$$

for $\{a,i\}, \{b,j\} = \{e,1\}, \{\mu,2\}, \{\tau,3\}$.[1] This provides us with simple, quantitative expressions of how the gaugino and higgsino contents of the charged lepton mass eigenstates (i.e., of the e, the μ, and the τ) affect the Z^0 leptonic decay widths. These effects, present when the μ_i are non-zero, can lead to non-universality among the Z^0 leptonic branching ratios or to mixed-flavor Z^0 leptonic decays.

Notice that the deviations of the Z^0 coupling coefficients are in fact proportional to $\mu_i \mu_j / M_0^2$, which must be small in this perturbative approximation (this tells us quantitatively what it means for the μ_i to be ''small''). In addition, the $\delta \widetilde{A}_{ab}^R$ are suppressed by the factor $m_i m_j / M_0^2$. Thus one might expect that the effects of the $\delta \widetilde{A}_{ab}^L$ will dominate those of the $\delta \widetilde{A}_{ab}^R$. However, the $\delta \widetilde{A}_{ab}^L$ are themselves proportional to $\cos^2 \beta$ which will strongly suppress their values in the large $\tan \beta$ regime (for example, $\cos^2 \beta \sim 10^{-3}$ for $\tan \beta = 45$). Neglecting terms proportional to $\cos \beta$ in the $\delta \widetilde{A}_{ab}^R$ (recall $\sin 2\beta$ is small when $\cos \beta$ is small), we find

$$\frac{\delta \widetilde{A}_{ab}^R}{\delta \widetilde{A}_{ab}^L} \simeq \frac{1}{2} (1 + \tan^2 \beta) \frac{m_i m_j}{M_0^2} \frac{M_2^2 [(M_2/M_W)^2 + 4]}{M_0^2}$$

$$\simeq \frac{1}{2} (1 + \tan^2 \beta) \frac{m_i m_j}{\mu_0^2} [(M_2/M_W)^2 + 4] \qquad (2.14)$$

(where the second expression holds for large $\tan \beta$ or $\mu_0 M_2 \gg M_W^2$). Thus if M_2 is large and $|\mu_0|$ is small, the effect of deviations from the SM for the right-hand compo-

nent of the Z^0-τ-τ coupling (and even the Z^0-τ-μ coupling) can be as significant as those for the left-hand component.

The Z^0 branching fraction into any pair of colorless charged fermions (with $M_Z > M_{\chi_a} + M_{\chi_b}$) is given by

$$Br(Z^0 \rightarrow \chi_a^+ \chi_b^-) = \frac{\alpha_2 \, \lambda^{1/2} \left(1, \dfrac{M_{\chi_a}^2}{M_Z^2}, \dfrac{M_{\chi_b}^2}{M_Z^2} \right)}{24 \cos^2 \theta_w} \frac{M_Z}{\Gamma_Z}$$

$$\times \left[1 - \frac{M_{\chi_a}^2 + M_{\chi_b}^2}{2 M_Z^2} - \frac{(M_{\chi_a}^2 - M_{\chi_b}^2)^2}{2 M_Z^4} \right. \\ \left. + \frac{6 M_{\chi_a} M_{\chi_b}}{M_Z^2} \frac{\widetilde{A}_{ab}^L \widetilde{A}_{ab}^R}{\widetilde{A}_{ab}^2} \right] \widetilde{A}_{ab}^2, \qquad (2.15)$$

where $\alpha_2 \equiv g_2^2 / 4\pi$ and

$$\widetilde{A}_{ab}^2 \equiv |\widetilde{A}_{ab}^L|^2 + |\widetilde{A}_{ab}^R|^2. \qquad (2.16)$$

The experimentally determined total decay width of the Z^0 is $\Gamma_Z = (2.4948 \pm 0.0075)$ GeV [12]. The kinematic λ-function is $\lambda(a,b,c) = (a-b-c)^2 - 4bc$. In the small μ_i perturbative approximation, and for $\tan \beta$ not too large, we have for the leptonic Z^0 decays,

$$\widetilde{A}_{ii}^2 \simeq (1 - 2 \sin^2 \theta_w)^2 + (4 \sin^4 \theta_w) + 2(1 - 2 \sin^2 \theta_w) \delta \widetilde{A}_{ii}^L$$

$$= .5027 + 2.148 \frac{M_W^2 \cos^2 \beta}{M_0^2} \left(\frac{\mu_i}{M_0} \right)^2, \qquad (2.17)$$

and

$$\widetilde{A}_{ab}^2 = |\delta \widetilde{A}_{ab}^L|^2 = \frac{4 M_W^4 \cos^4 \beta}{M_0^4} \left(\frac{\mu_i}{M_0} \right)^2 \left(\frac{\mu_j}{M_0} \right)^2 \quad (a,i \neq b,j). \qquad (2.18)$$

If $\tan \beta$ is large, then the right-hand component cannot be neglected, as noted above, and the $\widetilde{A}_{\tau\tau}^2$ and $\widetilde{A}_{\mu\tau}^2$ formulas should be modified to

$$\widetilde{A}_{\tau\tau}^2 \simeq (1 - 2 \sin^2 \theta_w)^2 + (4 \sin^4 \theta_w) + 2(1 - 2 \sin^2 \theta_w) \delta \widetilde{A}_{\tau\tau}^L$$

$$- 4 \sin^2 \theta_w \delta \widetilde{A}_{\tau\tau}^R$$

$$= .5027 + \left[2.148 \frac{M_W^2 \cos^2 \beta}{M_0^2} \right. \\ \left. - .926 \frac{m_3^2 (M_2^2 + 4 M_W^2) M_2^2}{M_0^6} \right] \left(\frac{\mu_3}{M_0} \right)^2, \qquad (2.19)$$

and

---

[1] In the formulas above and those that follow, index labels a and b are reserved for the physical mass eigenstates, $a,b = e, \mu, \tau$ (or the heavier charginos). Index labels i and j are used for basis state parameters in the single-VEV parametrization, $i,j = 1, 2,$ or 3. *In the small-μ_i approximation, a and i (or b and j) have a simple one-to-one correspondence. Hence, equations could be written with just one pair of index labels. However, both pairs will be kept to make clear that this is not true in general.*

$$\widetilde{A}^2_{\mu\tau} = |\delta\widetilde{A}^L_{\mu\tau}|^2 + |\delta\widetilde{A}^R_{\mu\tau}|^2$$

$$= \left[\frac{4M_W^4\cos^4\beta}{M_0^4} + \frac{m_2^2 m_3^2 (M_2^2 + 4M_W^2)^2 M_2^4}{M_0^{12}} \right]$$

$$\times \left(\frac{\mu_2}{M_0} \right)^2 \left(\frac{\mu_3}{M_0} \right)^2. \tag{2.20}$$

Note here that the numerical value $\sin^2\theta_w = 0.2315$ [12] has been used. This effective value for $\sin^2\theta_w$ absorbs the SM radiative corrections to the $Z^0 l_i l_i$ couplings. Note also that the two terms inside the bracket in Eq. (2.19) enter with opposite signs, implying that in some region of the parameter space, the deviation of $\Gamma(Z^0 \rightarrow \tau^+\tau^-)$ from the SM prediction could be suppressed by cancellation between these two terms even if μ_3 is quite substantial.

We now apply these results for couplings and branching ratios to specific processes in order to obtain limits on the μ_i.

A. Mixed-flavor leptonic Z^0 decays

For non-zero μ_i's, the Lagrangian of Eq. (2.4) leads to the tree-level flavor-violating Z^0 decays, $Z^0 \rightarrow e\mu$, $e\tau$, and $\mu\tau$. The predicted branching ratios for these decay modes are given by Eq. (2.15). The experimental bounds from LEP on these processes are shown in the third column of Table I. In the small-μ_i approximation, Eq. (2.18) translates these constraints into the following bounds:

$$\frac{|\mu_i\mu_j|}{M_0^2} \lesssim \mathcal{K}_{ij}(1 + \tan^2\beta)\frac{M_0^2}{M_W^2} \tag{2.21}$$

$$\mathcal{K}_{12} = 1.8 \times 10^{-3} \quad \text{from} \quad Z^0 \rightarrow e^\pm\mu^\mp$$

$$\mathcal{K}_{13} = 4.3 \times 10^{-3} \quad \text{from} \quad Z^0 \rightarrow e^\pm\tau^\mp$$

$$\mathcal{K}_{23} = 4.7 \times 10^{-3} \quad \text{from} \quad Z^0 \rightarrow \mu^\pm\tau^\mp.$$

Note that bounds apply to the products $|\mu_i\mu_j|$. That the constraints can be cast in such a simple form and in terms of so few RPV input parameters is a key strength of the single-VEV parametrization. Note also that the constraints become weaker as $\tan\beta$ increases.

B. Flavor-violating charged lepton decays

The $Z^0 l_i l_j$ couplings can also produce the tree-level FCNC decays of μ and τ via a virtual Z^0. These branching ratios are given by

$$Br(l_a^- \rightarrow l_b^- l_c^+ l_c^-) = \frac{\alpha_2^2\cos^4\beta}{1536\pi}\left(\frac{m_{l_a}}{M_Z}\right)^4\frac{m_{l_a}}{\Gamma_{l_a}}\widetilde{A}^2_{ab}\widetilde{A}^2_{cc} \tag{2.22}$$
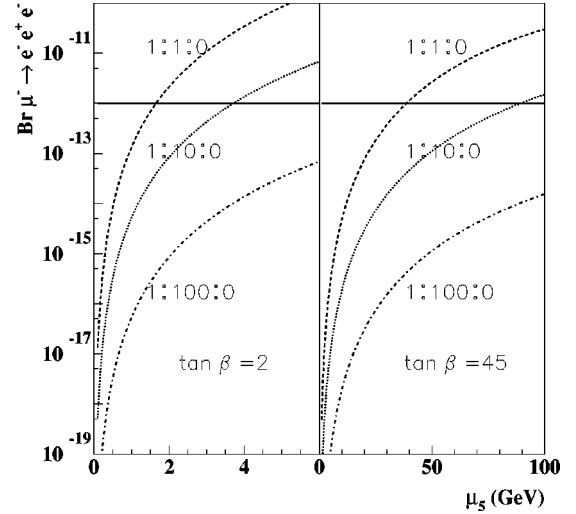

FIG. 1. Branching ratio for $\mu^- \rightarrow e^-e^+e^-$ as a function of μ_5 (in GeV), with $M_2 = \mu_0 = 200$ GeV and $\tan\beta = 2$ (left) or $\tan\beta = 45$ (right) for ratios of $\mu_1 : \mu_2 : \mu_3$ as marked. The solid horizontal line is the experimental bound. If μ_3 — here set to zero — is varied, it affects the curves only via μ_5, and hence stretches out the horizontal scale.

$$Br(l_a^- \rightarrow l_b^+ l_c^- l_c^-) = \frac{\alpha_2^2\cos^4\beta}{1536\pi}\left(\frac{m_{l_a}}{M_Z}\right)^4\frac{m_{l_a}}{\Gamma_{l_a}}(\widetilde{A}^2_{ac}\widetilde{A}^2_{bc}$$

$$+ |\widetilde{A}^L_{ac}|^2|\widetilde{A}^R_{bc}|^2 + |\widetilde{A}^R_{ac}|^2|\widetilde{A}^L_{bc}|^2), \tag{2.23}$$

where Γ_{l_a} is the total decay width and m_{l_a} the mass of the decaying l_a (masses of the daughter leptons are neglected). It is assumed the virtual intermediate is an off-shell Z^0; possible slepton-Higgs intermediates are assumed to be heavy and therefore to yield negligible contributions. Note from Eq. (2.23) that when the odd-flavored daughter lepton l_b has the charge opposite to the parent lepton, the branching ratio is suppressed by an extra factor of $\widetilde{A}^2_{ab}$ ($a \neq b$) compared to the case where the odd-flavor daughter lepton has the same sign as the parent. Actually, the latter case also has a contribution analogous to Eq. (2.23); however, this is insignificant relative to the Eq. (2.22) contribution.

The experimental limits on these decays are again given in the third column of Table I. Using Eq. (2.18) along with the lowest order value for $\widetilde{A}^2_{cc}$ ($= 0.5027$) from Eq. (2.17), bounds can be cast in the same form as in Eq. (2.21), with

$$\mathcal{K}_{12} = 1.4 \times 10^{-6} \quad \text{from} \quad \mu^- \rightarrow e^- e^+ e^-$$

$$\mathcal{K}_{13} = 4.5 \times 10^{-3} \quad \text{from} \quad \tau^- \rightarrow e^- \mu^+ \mu^-$$

$$\mathcal{K}_{12} = 4.3 \times 10^{-3} \quad \text{from} \quad \tau^- \rightarrow \mu^- e^+ e^-.$$

We see that while the τ decay constraints are comparable to the $Z^0 \rightarrow \tau l$ ($l = e$ or μ) constraints, the $\mu \rightarrow eee$ constraint is much more strict than that for $Z^0 \rightarrow e\mu$ due to the much stronger experimental bound on $\mu \rightarrow eee$. In Fig. 1, predicted values from the exact numerical calculation of this
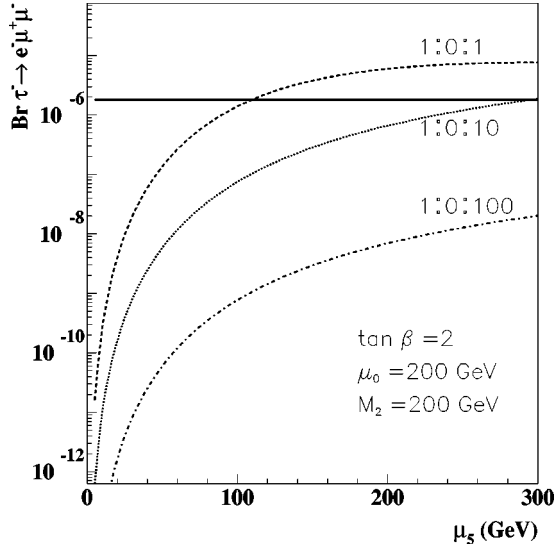
FIG. 2. Branching ratio for $\tau^- \to e^- \mu^+ \mu^-$ as a function of μ_5 (in GeV), with $M_2 = \mu_0 = 200$ GeV and $\tan\beta = 2$, for ratios of $\mu_1 : \mu_2 : \mu_3$ as marked. The solid horizontal line is the experimental bound. Here, μ_2 is set to zero; again, varying this stretches the horizontal scale.

branching ratio are shown as a function of the μ_i for the MSSM parameters $M_2 = \mu_0 = 200$ GeV and $\tan\beta = 2,45$. The constraint is very stringent for small $\tan\beta$ and remains relevant, although much weaker, even for large $\tan\beta$ (unlike the other constraints discussed so far). Plots for $Br(Z^0 \to e\mu)$ would look very similar except with a much weaker experimental bound. Note that in Fig. 1, the useful RPV parameter

$$\mu_5 \equiv \sqrt{\mu_1^2 + \mu_2^2 + \mu_3^2} \qquad (2.24)$$

is introduced to permit different $\mu_1 : \mu_2$ ratios to be plotted simultaneously. This parameter will appear repeatedly in subsequent discussions. Interpreted as a constraint on μ_5, Fig. 1 shows that the $\mu \to eee$ constraint can be evaded by supposing a strong hierarchy among the μ_i's (i.e., $\mu_1 \ll \mu_2 \ll \mu_3$), as can also be clearly seen from the approximate Eq. (2.21).

Figure 2 shows $Br(\tau^- \to e^- \mu^+ \mu^-)$ for $\tan\beta = 2$, again based on exact numerical calculations. There is no meaningful constraint for $\tan\beta = 45$ due to the much weaker experimental bound. We need not explicitly show results for the remaining processes: results for $Br(\tau^- \to e^- e^+ e^-)$ and $Br(\tau^- \to \mu^- \mu^+ \mu^-)$ are almost identical to Fig. 2, as are those for $Br(\tau^- \to \mu^- e^+ e^-)$ and $Br(\tau^- \to \mu^- \mu^+ \mu^-)$ if the roles of μ_1 and μ_2 are interchanged. Plots for $Br(Z^0 \to e\tau)$ and $Br(Z^0 \to \mu\tau)$ also yield very similar results. Note that in using Eq. (2.21) to obtain constraints on τ decays in the small μ_i approximation, extra contributions from $\tilde{A}^R_{\mu\tau}$ have been neglected. These $\tilde{A}^R_{\mu\tau}$ contributions are only significant at large $\tan\beta$, where constraints on μ_i from this process as given by Eq. (2.21) are superseded by limits from other processes. This is confirmed by exact numerical results. Finally, note also that for τ decays in which the odd-flavored daugh-
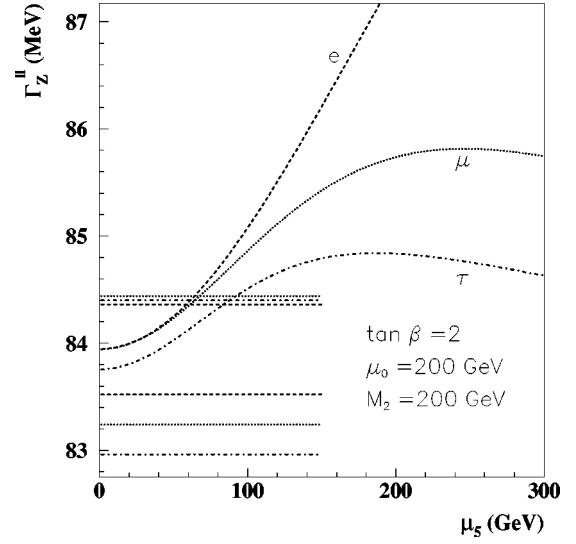

FIG. 3. Leptonic partial decay widths of the Z^0 (in MeV) as a function of μ_5 (in GeV), with $\mu_1 : \mu_2 : \mu_3 = 1 : 1 : 1$ [so that $\mu_i = (1/\sqrt{3})\mu_5$]; $M_2 = \mu_0 = 200$ GeV, and $\tan\beta = 2$. Horizontal lines at the left edge of the plot are the $\pm 3\sigma$ experimental bounds [11] for the corresponding quantities; they are independent of μ_5 and are truncated at right for clarity. Explicit values for the experimental bounds on these partial decay widths are found in [12].

ter lepton has the flipped charge, the result is proportional to $\tilde{A}^2_{e\mu}$ and thus very strongly limited by constraints from $Br(l_a^- \to l_b^- l_c^+ l_c^-)$ such that $Br(\tau^- \to l_b^+ l_c^- l_c^-) \lesssim 10^{-18}$.

C. Universality violations at the Z^0 peak

Equations (2.17) and (2.19) also produce deviations from SM predictions for $Br(Z^0 \to l_a l_a)$ which can break lepton universality. Figure 3 shows leptonic partial widths as a function of μ_5 for several choices of $\mu_1 : \mu_2 : \mu_3$, again using the representative MSSM parameter point $M_2 = \mu_0 = 200$ GeV and $\tan\beta = 2$. The experimental 3σ bounds are only exceeded for μ_5 values in excess of 50 GeV. As the value of μ_5 increases, the small-μ_i approximation loses its validity. The numerical results show that for sufficiently large μ_i values, the partial decay widths stop increasing as the μ_i's increase and in fact turn over and decrease. This behavior is common to all the decay widths discussed so far (although the maxima will in general occur at different μ_5 values, sometimes above the upper limits on the plots shown). This behavior can be understood via the "large μ_i" approximation employed in subsection E below to derive chargino masses. Note that if, at some point after reaching its maximum, the deviation in a partial width again drops below its experimental limit, then the large μ_5 values above this point are again acceptable. Thus it is possible that no upper bounds can be placed on μ_5 from these processes, but instead either only a finite range of μ_5 values is excluded or (if the maximum is too low) no μ_5 values are excluded at all. For further details, see [13]. In practice, other constraints will rule out arbitrarily large μ_5 values.

Universality constraints on $Z^0 \to l_a l_b$ decays are quantified via the observable $U_{br}^{(l_a l_b)}$ [14]:

$$U_{br}^{(l_a l_b)} \equiv \frac{\Gamma(Z^0 \to l_a^+ l_a^-) - \Gamma(Z^0 \to l_b^+ l_b^-)}{\Gamma(Z^0 \to l_a^+ l_a^-) + \Gamma(Z^0 \to l_b^+ l_b^-)}$$

$$= \frac{\tilde{A}_{aa}^2 - \tilde{A}_{bb}^2}{\tilde{A}_{aa}^2 + \tilde{A}_{bb}^2}$$

$$= 2.136 \frac{(\mu_i^2 - \mu_j^2) M_W^2 \cos^2\beta}{M_0^4}, \quad (2.25)$$

where the first equality follows from Eq. (2.4) and the second from Eq. (2.17). LEP experimental measurements on the partial widths can now be translated into the restrictions on the $U_{br}^{(l_a l_b)}$ listed in the third column of Table I. These are all compatible with the SM prediction of $U_{br}^{(l_a l_b)} = 0$, and, neglecting the (small) nonzero central values, translate into the following bounds on the μ_i:

$$\frac{1}{M_0^2} |\mu_i^2 - \mu_j^2| \lesssim \bar{\mathcal{K}}_{ij} (1 + \tan^2\beta) \frac{M_0^2}{M_W^2}. \quad (2.26)$$

The $\bar{\mathcal{K}}_{ij}$'s have values of $\bar{\mathcal{K}}_{12} = 2.05 \times 10^{-3}$, $\bar{\mathcal{K}}_{13} = 2.33 \times 10^{-3}$, and $\bar{\mathcal{K}}_{23} = 2.62 \times 10^{-3}$; they are comparable to the $\mathcal{K}_{ij}$'s of Eq. (2.21) obtained from flavor-violating Z^0 decays and τ decays. For large $\tan\beta$, deviations from the SM are highly suppressed; i.e., very high values of μ_5 (well beyond the range of validity of this approximation) are allowed. Exact numerical studies also confirm that these constraints vanish. Using the above formula from the small μ_i approximation, we find that μ_i's (or more precisely their difference in magnitudes) as large as M_0 become allowable for $\tan\beta \sim 20$. In fact, for large $\tan\beta$, Eq. (2.19) should be used for the $Z^0 \to \tau^+ \tau^-$ partial width. Cancellation among terms in this equation would further weaken any surviving $U_{br}^{(l_a \tau)}$ bound on μ_3.

D. Leptonic left-right asymmetry

Predictions for left-right asymmetries in Z^0 leptonic decays, which are defined by

$$\mathcal{A}_a \equiv \frac{|\tilde{A}_{aa}^L|^2 - |\tilde{A}_{aa}^R|^2}{|\tilde{A}_{aa}^L|^2 + |\tilde{A}_{aa}^R|^2} \quad (2.27)$$

follow immediately from Eqs. (2.17) and (2.19):

$$\mathcal{A}_a = \mathcal{A}_l^{(SM)} + 4.273 \frac{M_W^2 \cos^2\beta}{M_0^2} \left(\frac{\mu_j}{M_0}\right)^2 \quad (2.28)$$

(where $a = e, j = 1$ or $a = \mu, j = 2$),

$$\mathcal{A}_\tau = \mathcal{A}_l^{(SM)} + \left[4.273 \frac{M_W^2 \cos^2\beta}{M_0^2} \right.$$
$$\left. + 1.842 \frac{m_3^2 (M_2^2 + 4M_W^2) M_2^2}{M_0^6} \right] \left(\frac{\mu_3}{M_0}\right)^2. \quad (2.29)$$
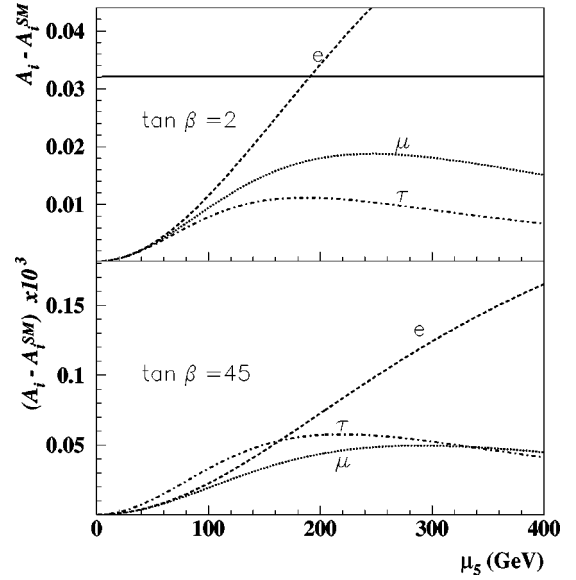

FIG. 4. Leptonic L-R asymmetry: deviations from SM predictions as functions of μ_5 (in GeV), with $\mu_1 : \mu_2 : \mu_3 = 1 : 1 : 1$ and $M_2 = \mu_0 = 200$ GeV for (a) $\tan\beta = 2$ and (b) $\tan\beta = 45$. The solid line approximates the experimental 3σ upper bounds for each of the 3 asymmetries.

First note that the $|\mu_i|$'s enter individually rather than in products or differences of two distinct $|\mu_i|$'s. This makes the left-right asymmetries potentially very useful in distinguishing effects from the three μ_i's. Note also that non-zero μ_i's always increase the $\mathcal{A}_a$'s from their SM values, and that the $\delta\tilde{A}_{\tau\tau}^R$ contribution now reinforces that of $\delta\tilde{A}_{\tau\tau}^L$. This could be important if these contributions cancel in $\tilde{A}_{\tau\tau}^2$ which enters into the previously discussed RPV τ effects. Another immediate consequence is that for the favored case of $\mu_3 > \mu_1$, $\mathcal{A}_\tau > \mathcal{A}_e$.

Equations (2.28) and (2.29) and conclusions drawn from them are valid in the small-μ_i approximation. In Fig. 4, the asymmetries are shown using exact numerical calculations (again for $M_2 = \mu_0 = 200$ GeV). For large values of μ_5, the $\mathcal{A}_a$'s cease rising with increasing μ_5, deviating from the approximate behavior of Eqs. (2.28) and (2.29). As with the Z^0 leptonic partial decay widths, a maximum is reached and then the slope turns negative. For low $\tan\beta$, this occurs for μ_5 values excluded for other reasons. But for high $\tan\beta$ it may occur in admissible regions of the parameter space. Also notice from Fig. 4 for $\tan\beta = 45$ that $\mathcal{A}_\tau$ shows an increase relative to $\mathcal{A}_e$ and $\mathcal{A}_\mu$ arising from the right-handed contribution.

Equations (2.28) and (2.29) require $\mathcal{A}_l^{(SM)}$ as input — this must be determined independent of the leptonic asymmetry measurements. Unfortunately, $\mathcal{A}_l^{(SM)}$ depends strongly on $\sin^2\theta_w$; for instance, $\mathcal{A}_l^{(SM)}$ decreases by more than 11% when $\sin^2\theta_w$ is increased by 1%. The effective value of $\sin^2\theta_w$ for the $Z^0 ll$ coupling depends on radiative corrections [15]; $\sin^2\theta_w = 0.2315$ employed here yields $\mathcal{A}_l^{(SM)} = 0.147$, but includes only SM corrections and not additional corrections depending upon SUSY parameters. Thus uncertainty in the effective value of $\sin^2\theta_w$ leads to even larger uncertainty

in $\mathcal{A}_l^{(SM)}$, which also includes beyond-SM contributions not apparent in the simple separations seen in the formulas above. In an attempt to reduce such uncertainties, Ref. [11] (following the idea put forward in Ref. [16]) suggests using

$$\Delta\mathcal{A}_{ab} \equiv \frac{\mathcal{A}_a - \mathcal{A}_b}{\mathcal{A}_a + \mathcal{A}_b} \qquad (2.30)$$

instead of the individual $\mathcal{A}_a$'s. $\Delta\mathcal{A}_{ab} = 0$ in the SM. In the small μ_i approximation, where $\mathcal{A}_a - \mathcal{A}_l^{(SM)}$ is also small,

$$\Delta\mathcal{A}_{ab} = \left(\frac{1}{\mathcal{A}_l^{(SM)}} - 1\right) U_{br}^{(l_a l_b)} \qquad (2.31)$$

(as noted in Ref. [11]), *if* $\delta\tilde{A}_{aa}^R$'s are neglected. If this is permissible, then the $\Delta\mathcal{A}_{ab}$ constraints have the same dependence on the μ_i's as the constraints for the $U_{br}^{(l_a l_b)}$, providing a compatibility condition for the RPV framework. The $\delta\tilde{A}_{aa}^R$'s may safely be neglected for the first two generations, meaning the allowed window for $\Delta\mathcal{A}_{e\mu}$ given in Table I follows immediately from that for $U_{br}^{(e\mu)}$ (though perhaps a small amount of extra widening to reflect the uncertainly in $\mathcal{A}_l^{(SM)}$ should be included). Unfortunately, the present experimental situation is far too imprecise for any incompatibility to be seen. As noted previously, $\delta\tilde{A}_{\tau\tau}^R$ may not be negligible, especially for larger $\tan\beta$. Adding these terms to $\Delta\mathcal{A}_{m\tau}$ and $U_{br}^{(l_m\tau)}$ means that the value of one is no longer determinable given only the value of the other. Furthermore, deviations from Eq. (2.31), which predicts $|\Delta\mathcal{A}_{m\tau}| \lesssim 0.03$, indicate a substantial contribution from $\delta\tilde{A}_{\tau\tau}^R$ (within the framework of the small-μ_i approximation).

In the τ case, then, since $U_{br}^{(l_a\tau)}$ experimental constraints cannot place bounds on the $\Delta\mathcal{A}_{a\tau}$'s, direct $\mathcal{A}_l$ measurements must be considered. These are listed in Table II and used to derive the 3σ bounds on the $\Delta\mathcal{A}_{a\tau}$'s shown in Table I. The $\mathcal{A}_e$ and $\mathcal{A}_\tau$ used in the $\Delta\mathcal{A}_{e\tau}$ bounds of Table I are obtained

TABLE II. Experimental left-right asymmetry results: $\mathcal{A}_i$ obtained from $\mathcal{A}_{FB}^l$ (using $\mathcal{A}_{FB}^l = \frac{3}{4}\mathcal{A}_e\mathcal{A}_l$) measured at LEP and SLD, $\mathcal{P}_\tau$ measured at LEP, and a direct measurement from SLD.

$\mathcal{A}_l$	Method	LEP combined [12]	SLD [17]
$\mathcal{A}_e$	FB	0.1461 ± 0.0110	$0.152 \pm .012$
	$\mathcal{P}_\tau$	$0.1399 \pm .0073$	—
	direct	—	$0.1543 \pm .0039$
$\mathcal{A}_\mu$	FB	$0.1488 \pm .0170$	$0.102 \pm .034$
$\mathcal{A}_\tau$	FB	$0.1753 \pm .0210$	$0.195 \pm .034$
	$\mathcal{P}_\tau$	$0.1411 \pm .0064$	—

from LEP measurements of τ polarization (note however that the SLD group at SLAC [17] measured $\mathcal{A}_e$ directly with their polarized electron beam and obtained a substantially higher value for $\mathcal{A}_e$). The $\Delta\mathcal{A}_{\mu\tau}$ bounds are obtained from LEP forward-backward asymmetry measurements (which provide the best $\mathcal{A}_\mu$ value but larger uncertainty in $\mathcal{A}_\tau$). Note that the bounds are considerably weaker than the 0.03 value given above, meaning that substantial deviation of $\mathcal{A}_\tau$ from $\mathcal{A}_l^{(SM)}$ (including a potentially important contribution from $\delta\tilde{A}_{\tau\tau}^R$) is possible.

E. Limits on charginos

We now turn to constraints associated with the remaining color-singlet charged fermions, the charginos. The term ''chargino'' is here applied to the two (heaviest) mass eigenstates remaining after the other three eigenstates in Eq. (2.3) are fixed to give the ''leptons'' with well-known experimentally observed masses ($\bar{m}_1 = m_e$, $\bar{m}_2 = m_\mu$, $\bar{m}_3 = m_\tau$). In the MSSM, the charginos have masses given by M_{c1} and M_{c2} in Eq. (2.7). For nonzero values of the μ_i, the chargino masses are modified to $\bar{M}_{c1}$ and $\bar{M}_{c2}$ in Eq. (2.3). If the μ_i are ''small,'' then $\bar{M}_{c1} \simeq M_{c1}$ and $\bar{M}_{c2} \simeq M_{c2}$; however, larger values of the μ_i's can produce more pronounced effects. From Eq. (2.8),

$$\mathcal{M}_{\mathcal{C}}(\mathcal{M}_{\mathcal{C}})^\dagger = \begin{bmatrix} \frac{g^2 v_u^2}{2} + M_2^2 & \frac{g v_d}{\sqrt{2}} M_2 + \frac{g v_u}{\sqrt{2}} \mu_0 & \frac{g v_u}{\sqrt{2}} \mu_1 & \frac{g v_u}{\sqrt{2}} \mu_2 & \frac{g v_u}{\sqrt{2}} \mu_3 \\ \frac{g v_d}{\sqrt{2}} M_2 + \frac{g v_u}{\sqrt{2}} \mu_0 & \frac{g^2 v_d^2}{2} + \mu_0^2 & \mu_0\mu_1 & \mu_0\mu_2 & \mu_0\mu_3 \\ \frac{g v_u}{\sqrt{2}} \mu_1 & \mu_0\mu_1 & m_1^2 + \mu_1^2 & \mu_1\mu_2 & \mu_1\mu_3 \\ \frac{g v_u}{\sqrt{2}} \mu_2 & \mu_0\mu_2 & \mu_1\mu_2 & m_2^2 + \mu_2^2 & \mu_2\mu_3 \\ \frac{g v_u}{\sqrt{2}} \mu_3 & \mu_0\mu_3 & \mu_1\mu_3 & \mu_2\mu_3 & m_3^2 + \mu_3^2 \end{bmatrix}. \qquad (2.32)$$

Now by applying the rotation

$$\begin{pmatrix} I_{2\times2} & 0 \\ 0 & R_5 \end{pmatrix} \quad \text{where} \quad R_5^\dagger \begin{pmatrix} \mu_1 \\ \mu_2 \\ \mu_3 \end{pmatrix} = \begin{pmatrix} \mu_5 \\ 0 \\ 0 \end{pmatrix}$$

and μ_5 is given by Eq. (2.24), $\mathcal{M}_C(\mathcal{M}_C)^\dagger$ can be rotated into the form

$$\begin{bmatrix} \frac{g^2 v_u^2}{2} + M_2^2 & \frac{g v_d}{\sqrt{2}} M_2 + \frac{g v_u}{\sqrt{2}} \mu_0 & \frac{g v_u}{\sqrt{2}} \mu_5 & 0 & 0 \\ \frac{g v_d}{\sqrt{2}} M_2 + \frac{g v_u}{\sqrt{2}} \mu_0 & \frac{g^2 v_d^2}{2} + \mu_0^2 & \mu_0 \mu_5 & 0 & 0 \\ \frac{g v_u}{\sqrt{2}} \mu_5 & \mu_0 \mu_5 & \mu_5^2 & 0 & 0 \\ 0 & 0 & 0 & 0 & 0 \\ 0 & 0 & 0 & 0 & 0 \end{bmatrix} + \begin{bmatrix} 0_{2\times2} & & 0 \\ & & \\ 0 & R_5^\dagger \begin{pmatrix} m_1^2 & 0 & 0 \\ 0 & m_2^2 & 0 \\ 0 & 0 & m_3^2 \end{pmatrix} R_5 \end{bmatrix}. \quad (2.33)$$

The matrix R_5 will appear again in the next section when the color-singlet neutral fermions are considered. In the limit where $\mu_5 \gg m_3 \simeq m_\tau$ (referred to henceforth as the large μ_i approximation[2]), the second matrix of expression (2.33) that is proportional to the m_i's may be dropped. This leads to simple analytic formulas for the chargino mass eigenvalues:

$$\bar{M}_{c1,c2}^2 = \frac{1}{2}[M_2^2 + 2M_W^2 + \mu_0^2 + \mu_5^2] \pm \frac{1}{2}[(\mu_0^2 + \mu_5^2 - M_2^2 - 2M_W^2 \cos 2\beta)^2 + 8M_W^2 (M_2 \sin\beta + \mu_0 \cos\beta)^2]^{1/2} \quad (2.34)$$

$$= \frac{1}{2}(\bar{\alpha}_1 + \bar{\alpha}_2) \pm \frac{1}{2}\sqrt{(\bar{\alpha}_1 - \bar{\alpha}_2)^2 + 2(g v_u M_2 + g v_d \mu_0)^2} \quad (2.35)$$

$$= \frac{1}{2}[M_{c1}^2 + M_{c2}^2 + \mu_5^2] \pm \frac{1}{2}[(M_{c2}^2 - M_{c1}^2 - \mu_5^2)^2 - 4\mu_5^2 \cos^2\theta_R (M_{c2}^2 - M_{c1}^2)^2]^{1/2} \quad (2.36)$$

where

$$\bar{\alpha}_1 \equiv \frac{g v_u^2}{2} + \mu_0^2 + \mu_5^2 \quad \text{and} \quad \bar{\alpha}_2 \equiv \frac{g v_d^2}{2} + M_2^2. \quad (2.37)$$

Within this approximation the chargino masses only depend on the μ_i through the single parameter μ_5. The roles of μ_0 and μ_5 in the mass formulas are very similar. Note from Eq. (2.36) that the chargino masses reduce to the MSSM chargino masses when $\mu_5 = 0$. Also note that a non-zero value for μ_5 *increases* the lighter chargino mass; hence, some region of the $M_2 - \mu_0$ parameter space that is ruled out in the MSSM by the chargino mass bound [18] can be reinstated when $\mu_5 \neq 0$. However, correct chargino mass bounds for RPV scenarios require analysis of the decay modes. One such analysis was recently performed for a specific bilinear RPV model [19]; a general analysis in the single-VEV parametrization, including contributions from both bilinear and trilinear RPV couplings, is currently in progress.
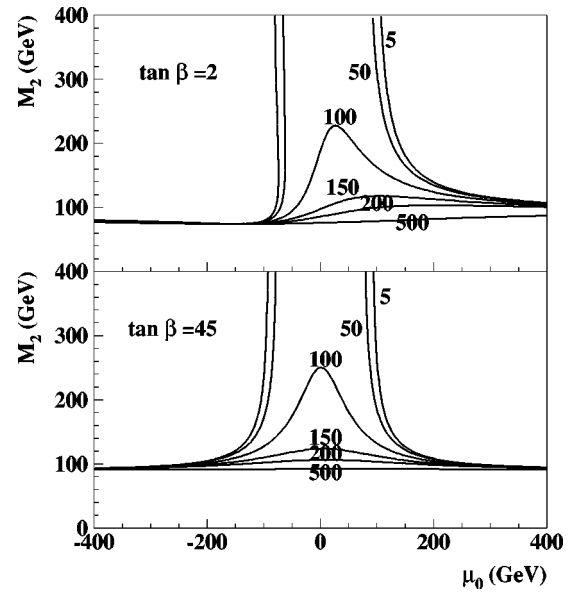

FIG. 5. Chargino masses. Contours show minimum values of μ_5 (in GeV) necessary to push the lighter chargino mass above 90 GeV for (a) $\tan\beta = 2$ and (b) $\tan\beta = 45$. The region above or outside a given contour has $\bar{M}_{c1} > 90$ GeV for μ_5 at or above the designated value.

_____

[2]Note that this is *not* the converse of the small μ_i approximation, which requires $\mu_i \ll M_0$.

It is possible to simultaneously have $\mu_5 \gg m_\tau$ and $\mu_i \ll M_0$, meaning that both the ''large-μ_i'' and the ''small-μ_i'' approximations will yield quite accurate results. In fact, results from the two methods agree well with each other and with the exact numerical results in most relevant regions of the parameter space. Using the exact numerical calculation, the region in MSSM parameter space that would be excluded by a 90 GeV chargino mass bound is plotted in Fig. 5, from which it is clear that constraints based on such an analysis will be significant if M_2 and/or μ_0 are small.

Bounds from Z^0 decays into two charginos or a chargino and a lepton follow from the general formula for Z^0 decays into a pair of charged fermions, Eq. (2.4). However, determining the exact values for these bounds requires detailed information about chargino decays from detector simulations which is beyond the scope of this work. Therefore, only a conservative bound is applied: Z^0 decays involving at least one (on-shell) chargino are required to have branching ratios of less than 10^{-5} (as noted in Table I).

Turning to the lepton sector, we see that in the limit where $m_i^2 = 0$, the matrix $\mathcal{M}_C(\mathcal{M}_C)^\dagger$ of Eq. (2.32) [or Eq. (2.33)] has three zero eigenvalues. Thus, in this approximation, the masses of the physical leptons are zero. Despite this degen-

eracy, the correct eigenvectors can be found by requiring that they do not differ significantly from the exact massive eigenstates obtained when the non-zero m_i are retained *if μ_5^2 is large*. Three such massless eigenvectors for $\mathcal{M}_C(\mathcal{M}_C)^\dagger$ with $m_i^2 = 0$ are given by

$$|l_1'\rangle = \left(\frac{gv_d}{\sqrt{2}}\mu_1, -M_2\mu_1, M_0^2, 0, 0 \right)^T \Big/ \Delta_1$$

$$|l_2'\rangle = \left(\frac{gv_d}{\sqrt{2}}\mu_2, -M_2\mu_2, 0, M_0^2, 0 \right)^T \Big/ \Delta_2$$

$$|l_3'\rangle = \left(\frac{gv_d}{\sqrt{2}}\mu_3, -M_2\mu_3, 0, 0, M_0^2 \right)^T \Big/ \Delta_3$$

$$(2.38)$$

(the $\Delta_i \equiv \sqrt{M_0^4 + \bar{\alpha}_2\mu_i^2}$ are normalization constants). Since these are degenerate states, any linear combination of the three will be a massless eigenstate. The natural hierarchy of the m_i values ($m_3 > m_2 > m_1$) requires the following choice of orthogonal eigenvectors:

$$|l_e\rangle \propto |l_1'\rangle = \left(\frac{gv_d}{\sqrt{2}}\mu_1, -M_2\mu_1, M_0^2, 0, 0 \right)^T \Big/ \Delta_e$$

$$|l_\mu\rangle \propto |l_2'\rangle - |l_1'\rangle\langle l_1'|l_2'\rangle = \left(\frac{gv_d}{\sqrt{2}}\mu_2, -M_2\mu_2, -\bar{\alpha}_2\mu_2\mu_1/M_0^2, \Delta_e^2/M_0^2, 0 \right)^T M_0^2 \Big/ (\Delta_e\Delta_\mu)$$

$$|l_\tau\rangle \propto |l_3'\rangle - |l_1'\rangle\langle l_1'|l_3'\rangle - |l_2'\rangle\langle l_2'|l_3'\rangle = \left(\frac{gv_d}{\sqrt{2}}\mu_3, -M_2\mu_3, -\bar{\alpha}_2\mu_3\mu_1/M_0^2, -\bar{\alpha}_2\mu_3\mu_2/M_0^2, \Delta_\mu^2/M_0^2 \right)^T M_0^2 \Big/ (\Delta_\mu\Delta_\tau)$$

$$(2.39)$$

where the normalization constants are

$$\Delta_e \equiv \sqrt{M_0^4 + \bar{\alpha}_2\mu_1^2}, \quad \Delta_\mu \equiv \sqrt{M_0^4 + \bar{\alpha}_2(\mu_1^2 + \mu_2^2)},$$

$$\Delta_\tau \equiv \sqrt{M_0^4 + \bar{\alpha}_2(\mu_1^2 + \mu_2^2 + \mu_3^2)}. \tag{2.40}$$

The first components of these three vectors are the elements U_L^{a1} of the left rotation matrix in Eq. (2.3):

$$U_L^{e1} = \frac{gv_d}{\sqrt{2}}\frac{\mu_1}{\Delta_e}; \quad U_L^{\mu1} = \frac{gv_d}{\sqrt{2}}\frac{\mu_2 M_0^2}{\Delta_e\Delta_\mu}; \quad U_L^{\tau1} = \frac{gv_d}{\sqrt{2}}\frac{\mu_3 M_0^2}{\Delta_\mu\Delta_\tau}. \tag{2.41}$$

These quantities appear in the expression for the anomalous coupling coefficients $\delta\tilde{A}_{ab}^L$ of Eq. (2.5). Note that in the limit $\mu_i \to 0$, $\Delta_a \to M_0^2$ and we recover the ''small μ_i'' approximation results given by Eqs. (2.10). The dependence of the normalization constants (the Δ_a's) on the μ_i's indicates that

the decay widths will *decrease* (for μ and τ) as the μ_i's increase, and exposes the reason behind the maxima seen in Figs. 3 and 4. Thus if an experimental bound actually allows the maximum value (for instance at large $\tan\beta$ where there is strong suppression), then that bound may provide no constraint on μ_5 (or equivalently on the μ_i's) at all. Even if the maximum is excluded, a window of large (possibly *very* large) μ_i's may be allowed. However, this region of the RPV parameter space is largely ruled out by limits on neutrino masses and bounds from neutrino scattering and charged current processes. Therefore we do not consider very large μ_i values further at present and instead proceed to a discussion of these additional constraints.

III. COLOR-SINGLET NEUTRAL FERMIONS

In the single-VEV parametrization, the Lagrangian terms contributing to the color-singlet neutral fermion (neutrino and neutralino) masses may be written as

$$\mathcal{L} \ni -(i\lambda_0^C \quad i\lambda_3^C \quad \tilde{h}_u^{0\,C} \quad \tilde{h}_d^{0\,C} \quad \nu_1^C \quad \nu_2^C \quad \nu_3^C)$$
$$\times \mathcal{M}_{\mathcal{N}}(-i\lambda_0 \quad -i\lambda_3 \quad \tilde{h}_u^0 \quad \tilde{h}_d^0 \quad \nu_1 \quad \nu_2 \quad \nu_3)^T$$
$$+ \text{c.c.}, \tag{3.1}$$

where $\tilde{h}_u^0$, $\tilde{h}_d^0$, and ν_i ($i=1-3$) are the Dirac spinors associated with the neutral superfields in $\hat{H}_u$, $\hat{L}_0$, and $\hat{L}_i$, respectively, of Eq. (1.3) and $-i\lambda_0$ and $-i\lambda_3$ are, respectively, the B-ino and w-ino components. C refers to charge conjugation acting on each spinor. Since neutrinos are assumed to have zero Yukawa masses, the same R_5 rotation that was used when the Yukawa masses for the charged leptons were neglected is also applicable to $\mathcal{M}_{\mathcal{N}}$. Now there is no approximation, no Yukawa part to throw away; two massless neutrino states decouple [20], leaving a 5×5 matrix:

$$\mathcal{M}_{\mathcal{N}} = \begin{vmatrix} M_1 & 0 & \frac{g'v_u}{2} & -\frac{g'v_d}{2} & 0 & 0 & 0 \\ 0 & M_2 & -\frac{gv_u}{2} & \frac{gv_d}{2} & 0 & 0 & 0 \\ \frac{g'v_u}{2} & -\frac{gv_u}{2} & 0 & -\mu_0 & -\mu_1 & -\mu_2 & -\mu_3 \\ -\frac{g'v_d}{2} & \frac{gv_d}{2} & -\mu_0 & 0 & 0 & 0 & 0 \\ 0 & 0 & -\mu_1 & 0 & 0 & 0 & 0 \\ 0 & 0 & -\mu_2 & 0 & 0 & 0 & 0 \\ 0 & 0 & -\mu_3 & 0 & 0 & 0 & 0 \end{vmatrix} \overset{R_5}{\Rightarrow} \begin{pmatrix} M_1 & 0 & \frac{g'v_u}{2} & -\frac{g'v_d}{2} & 0 \\ 0 & M_2 & -\frac{gv_u}{2} & \frac{gv_d}{2} & 0 \\ \frac{g'v_u}{2} & -\frac{gv_u}{2} & 0 & -\mu_0 & -\mu_5 \\ -\frac{g'v_d}{2} & \frac{gv_d}{2} & -\mu_0 & 0 & 0 \\ 0 & 0 & -\mu_5 & 0 & 0 \end{pmatrix}. \tag{3.2}$$

A. Neutrino mass (tree level)

The single massive neutrino that results from diagonalizing this tree-level mixing matrix was discussed in the first paper in this series [5]. Here again we denote the massive state by $|\nu_5\rangle = (\mu_1/\mu_5)|\nu_1\rangle + (\mu_2/\mu_5)|\nu_2\rangle + (\mu_3/\mu_5)|\nu_3\rangle$. Approximate analytic formulas for its mass were found to be

$$m_{\nu_5} = -\frac{1}{2}\frac{\mu_5^2 v^2 \cos^2\beta(xg^2+g'^2)}{\mu_0[2xM_2\mu_0 - (xg^2+g'^2)v^2 \sin\beta\cos\beta]} \tag{3.3}$$

(where $v^2 \equiv v_u^2 + v_d^2$ and $M_1 = xM_2$; $x = \frac{5}{3}\tan^2\theta_w$ assuming gaugino unification, as is done in all numerical calculations) from a "seesaw" approximation in which μ_5 is taken to be small and

$$m_{\nu_5} = -\frac{1}{4}\frac{\mu_5^2 v^2 \cos^2\beta(xg^2+g'^2)}{(\mu_0^2+\mu_5^2)xM_2} \tag{3.4}$$

from a perturbative treatment in which the electroweak symmetry breaking terms are regarded as small but the magnitude of μ_5 is not restricted. Key features to note are:

The mass has a simple dependence on only one RPV parameter, μ_5. This is to be contrasted with results found without using the single-VEV parametrization [21]. The formulas above are also quite general. In particular, the trilinear terms have *not* been set to zero—they simply do not contribute to the tree-level mass formulas. They will reappear at the one-loop level; however, loop effects are expected to be small compared to those at the tree level [22].

The approximate expressions, Eqs. (3.3) and (3.4), indicate that the neutrino mass is proportional to μ_5^2 if $\mu_5 \ll \mu_0$. Equation (3.4) also shows that for $\mu_5 \gg \mu_0$, the neutrino mass approaches a constant asymptotic value. The features of these approximate formulas are confirmed by exact numerical calculations, as shown in Fig. 6 for the MSSM parameters $M_2 = \mu_0 = 200$ GeV and $\tan\beta = 2.45$. Note in particular the linear rise in $\log m_{\nu_5}$ seen in the log-log inserts for low $\log\mu_5$ values, as expected if $m_{\nu_5} \propto \mu_5^2$. Note also that there is no decrease in m_{ν_5} for high μ_5 values, in contrast to the case of several constraints in the previous section. Therefore, unless the asymptotic value falls below the experimental bound, the μ_5 upper limit from m_{ν_5} will close any large-μ_5 window.

There is strong suppression both at high $\tan\beta$ due to the $\cos^2\beta$ factor[3] and at high M_2. Inverting Eq. (3.4) yields a bound on μ_5:

$$\mu_5^2 < \frac{4x\mu_0^2 M_2 m_{\nu_{(\text{bound})}}}{v^2\cos^2\beta(xg^2+g'^2) - 4xM_2 m_{\nu_{(\text{bound})}}}, \tag{3.5}$$

---

[3]This factor was also obtained in [23], but additional assumptions led to compensating factors that canceled the suppression.
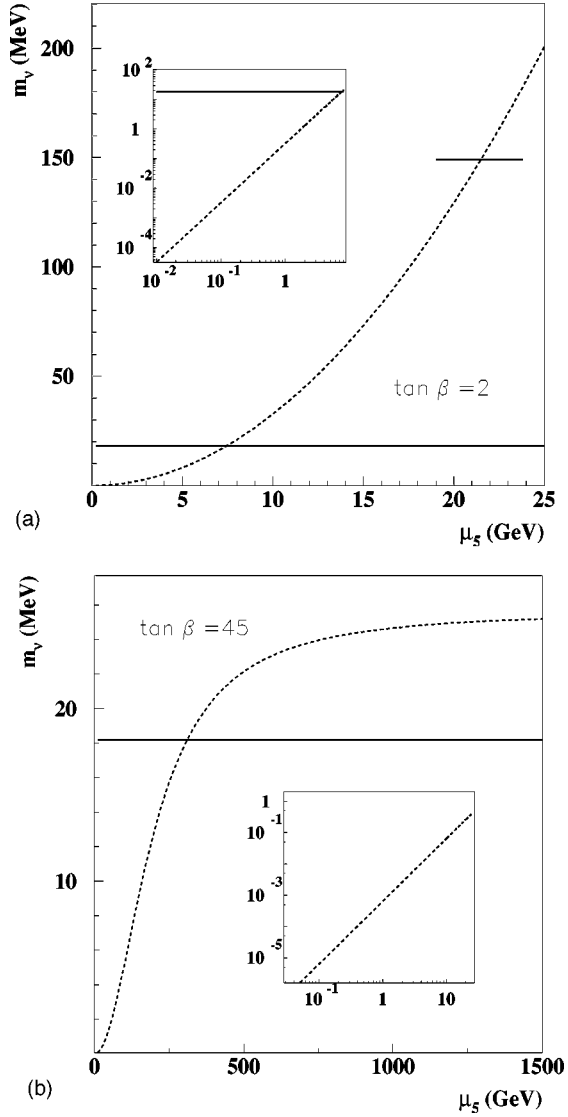
(a)

(b)

FIG. 6. Neutrino mass m_{ν_5} as a function of μ_5 (in GeV), with $M_2 = \mu_0 = 200$ GeV and (a) $\tan\beta = 2$, (b) $\tan\beta = 45$. The lower horizontal line is the 18.2 MeV machine bound for a pure ν_τ; the upper horizontal line is the 149 MeV bound for a generic ν_5. ($M_1 = xM_2$, with $x = \frac{5}{3}\tan^2\theta_w$.) Insets: Low μ_5 portion of curve on log-log scale.

FIG. 7. Maximum allowed values of μ_5 (in GeV) consistent with neutrino mass bounds: machine bound $m_{\nu_\tau} < 18.2$ MeV (applicable for $\mu_1:\mu_2:\mu_3 = 0:0:1$) for (a) $\tan\beta = 2$ and (b) $\tan\beta = 45$; the absolute bound $m_{\nu_5} < 149$ MeV for (c) $\tan\beta = 2$ and (d) $\tan\beta = 45$. The region below or inside of a given contour is excluded for μ_5's above the indicated value.

clearly demonstrating the high $\tan\beta$ suppression. The exact numerical results in both Figs. 6a and 6b and Figs. 7b and 7d also illustrate that the asymptotic limit is much lower for large $\tan\beta$. In addition, as M_2 increases, the denominator goes to zero, beyond which μ_5 is unconstrained.

If we assume $\mu_5 = \mu_3 \Leftrightarrow (\mu_1:\mu_2:\mu_3) = (0:0:1)$, then the recently improved mass bound on ν_τ from LEP, $\nu_\tau < 18.2$ MeV [24] (shown by solid horizontal lines in Figs. 6,ab), implies that, for $\tan\beta = 45$, there is no m_{ν_τ} constraint on μ_5 when $M_2 \gtrsim 280$ GeV (Fig. 7b). Analogous arguments can be made for $\mu_5 = \mu_1$ and $\mu_5 = \mu_2$ using $m_{\nu_e} < 5$ eV [25] and $m_{\nu_\mu} < 170$ keV [26], respectively. Due to the much tighter bounds these constraints exclude all interesting regions of parameter space *with such* $(\mu_1:\mu_2:\mu_3)$ *ratios*.
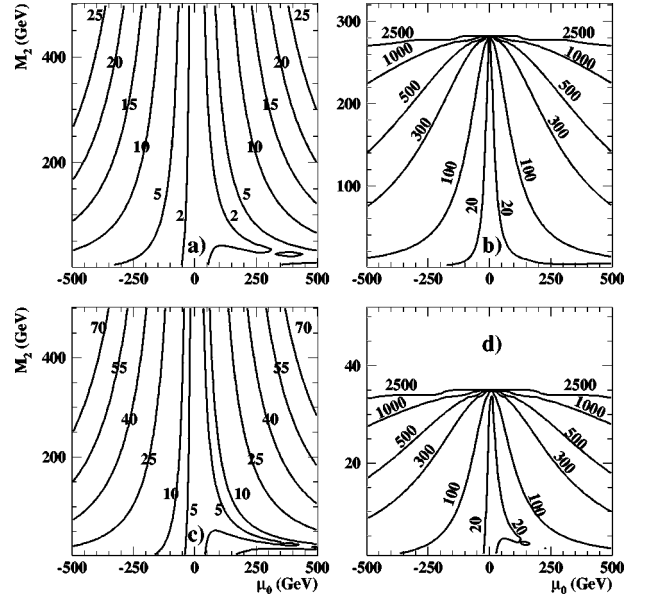
The negative sign for the neutrino mass in Eqs. (3.3) and (3.4) can be removed by redefining the fields in Eq. (3.1) (see [27] for more details).

If more than one of the μ_i's is non-zero, then the massive neutrino will be an admixture of the three neutrino basis states plus (especially for large μ_i's) the two gaugino and two Higgsino states. Using the matrix U_0 to diagonalize $\mathcal{M_N}$, the eigenvalues are

$$U_0^\dagger \mathcal{M_N} U_0 = \mathrm{diag}\{M_{n1}, M_{n2}, M_{n3}, M_{n4}, 0, 0, m_{\nu_5}\}, \quad (3.6)$$

where the massive neutrino is defined to be the lightest of the massive states and the four heavier states are termed neutralinos.[4] Further, note that there is no reason to expect alignment between the neutrino eigenstates and the charged lepton mass eigenstates (e, μ, and τ). Neutrino mass bounds in this more general case are more complicated, and better constraints are in fact obtainable from analysis of charged current processes (to be discussed in detail in the next section) than from direct mass bounds on ν_τ (or ν_μ) [30]. Based on such an analysis, Bottini *et al.* [31] gave a general neutrino mass bound of 149 MeV for a massive neutrino that was an admixture of ν_e, ν_μ, and ν_τ. The present

_____

[4]Going beyond the tree level will give small masses to the two zero mass neutrino eigenstates found here. Trilinear RPV terms will contribute to these corrections. Attempts to fit sub-eV mass neutrinos such as suggested by results of the Super-Kamiokande experiment [28] into the RPV framework will require knowledge of these corrections. This is beyond the scope of the present work. See [29] for more details.

case differs from theirs since in the RPV framework the massive neutrino can also have gaugino and Higgsino contributions. Nonetheless, the 149 MeV mass bound is in fact applicable as will be justified in the following section treating charged current interactions. This bound is shown in Fig. 6a as the upper horizontal line, but not shown for the $\tan \beta = 45$ case depicted in Fig. 6b since the bound is never reached.

Cosmological neutrino mass bounds also exist. These are usually far more stringent than the neutrino mass bounds discussed thus far, and upper limits of $m_\nu \lesssim 35$ eV have been given [32]. However, additional assumptions about cosmology enter when determining these values, which are also sensitive to the decay modes of the massive neutrino, which is expected to be unstable. Due to these loopholes, a MeV neutrino is not cosmologically taboo [33].

Upper bounds on μ_5 (obtained from exact numerical calculations) throughout the μ_0-M_2 MSSM parameter space are shown for $\tan \beta = 2,45$ in Fig. 7. Figures 7a,b show results assuming a mass bound of 18.2 MeV—i.e., assuming $(\mu_1 : \mu_2 : \mu_3) = (0:0:1)$ (these update the plots of [5] which assumed a mass bound of 24 MeV for ν_τ); and Figs. 7c,d show results with the more general bound of 149 MeV. Bounds on μ_5 weaken as either M_2 and/or $|\mu_0|$ increase. As noted in [5], for high $\tan \beta$, μ_5 values in the hundreds of GeV are permitted by the ν_τ mass bound.

B. Invisible Z^0 width

The couplings of the seven Majorana mass eigenstates to the Z^0 boson are given by

$$\mathcal{L}_{\chi^0 \chi^0 Z^0} = -\frac{g_2}{4 \cos \theta_w} \chi_c^0 \gamma_\mu (i \, \text{Im} \, \widetilde{C}_{cd} - \gamma_5 \text{Re} \, \widetilde{C}_{cd}) \chi_d^0 Z^\mu,$$

(3.7)

where $\widetilde{C}_{cd} = \widetilde{C}_{cd}^\dagger = (U_0 T^Z U_0^\dagger)_{cd}$ and $T^Z = \text{diag}(0, 0, -1, 1, 1, 1, 1)$ (again adopting the notation of [11]). The partial Z^0 decay width into a pair of neutral fermions (with $M_Z > M_{\chi_c} + M_{\chi_d}$) is then given by

$$\Gamma(Z^0 \rightarrow \bar{\chi}_c^0 \chi_d^0) = \frac{\alpha_2 \, \lambda^{1/2} \left(1, \frac{M_{\chi_c}^2}{M_Z^2}, \frac{M_{\chi_d}^2}{M_Z^2} \right)}{12 \cos_w^{2\theta}} \left[1 - - \frac{M_{\chi_c}^2 + M_{\chi_d}^2}{2 M_Z^2} \right.$$
$$\left. - \frac{(M_{\chi_c}^2 - M_{\chi_d}^2)^2}{2 M_Z^4} - \frac{3 M_{\chi_c} M_{\chi_d}}{M_Z^2} \right] |\widetilde{C}_{cd}|^2.$$

(3.8)

In the SM, the invisible Z^0 width, $\Gamma_{Z_{inv}}^{SM}$, is given by the sum of the partial decay widths of the Z^0 into the massless neutrinos. From this width, the number of SM neutrino flavors has been measured to be 3.09 ± 0.13 [25]. In the R-parity conserving MSSM, the decay of the Z^0 into a pair of the stable lightest neutralinos (taken as the LSP's) should
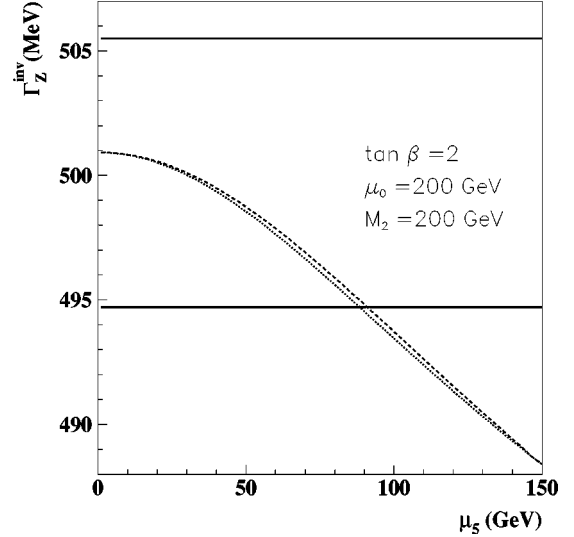

FIG. 8. The invisible Z^0-width (in MeV) as a function of μ_5 (in GeV), with $M_2 = \mu_0 = 200$ GeV and $\tan \beta = 2$. The solid horizontal lines are the upper and lower experimental bounds. $\Gamma_{Z_{inv}}^{RPV}$ is assumed to be $\Gamma(Z^0 \rightarrow \nu_c \nu_d)$ (dotted curve) or $\Gamma(Z^0 \rightarrow \nu_c \nu_d, \nu_c \chi_1^0, \chi_1^0 \chi_1^0)$ (dashed curve) where χ_1^0 is the lightest neutralino (4th lightest neutral color-singlet fermion).

also be included[5], meaning that $\Gamma_{Z_{inv}}^{MSSM} \geqslant \Gamma_{Z_{inv}}^{SM}$. When R-parity violation is permitted, the situation becomes more complicated. $\Gamma(Z^0 \rightarrow \nu_5 \nu_5)$ is suppressed by kinematic factors for the now massive neutrino. The Z^0 coupling may also change due to gaugino and Higgsino contributions to ν_5. Further, whether or not the partial decay width to the massive neutrino or to any of the more massive neutralinos should be included in $\Gamma_{Z_{inv}}^{RPV}$ will depend on how these particles decay.[6] As a result, $\Gamma_{Z_{inv}}^{RPV}$ need not be larger than $\Gamma_{Z_{inv}}^{SM}$. An example of this is shown in Fig. 8, where $\Gamma_{Z_{inv}}^{RPV}$ is plotted for the generic parameter space point $M_2 = \mu_0 = 200$ GeV and $\tan \beta = 2$ assuming contributions from the two massless neutrinos and ν_5 (dotted curve) and from the two massless neutrinos, ν_5, and the lightest of the neutralinos (dashed curve). Since the LEP measurement of $\Gamma_{Z_{inv}}$ given in Table I is slightly below the SM value, the RPV framework can actually give better agreement. The solid horizontal lines in Fig. 8 give the 3σ bounds for the LEP measurement. These do not pose a strong constraint on μ_5, allowing values

---

[5]Other contributions may also have to be included — such as Z^0 decays to the second lightest neutralino which in turn decays to the lightest neutralino and a pair of neutrinos; or Z^0 decays to sparticles which are close in mass to the LSP and thus produce decay products too soft to detect when they in turn decay to the LSP. These effects will always *increase* $\Gamma_{Z_{inv}}^{MSSM}$.

[6]Light scalar states might also contribute to the $\Gamma_{Z_{inv}}^{RPV}$, either directly or as virtual propagators. This further complicates the situation due to the larger number of free parameters in the RPV scalar sector. We make the reasonable assumption here that such scalar states are too heavy to make meaningful contributions.

up to ~ 100 GeV in this case, as compared to the neutrino mass constraint which from Fig. 7c demands $\mu_5 \lesssim 21.5$ GeV for $m_{\nu_5} < 149$ MeV. A thorough study of the decay modes of the massive neutrino as well as the other particle states in the model is necessary to make more definitive predictions. Such input will also be required if we wish to constrain this minimal RPV model using the full Z^0 width and the searches for anomalous Z^0 decays, such as to neutralinos ($Z^0 \to \chi_i^0 \chi_j^0, \chi_j^0 \nu; j \neq 1$).

IV. CHARGED CURRENT INTERACTIONS

Up to this point, color-singlet fermion interactions with on- and off-shell Z^0 bosons have been analyzed. Important constraints can also be obtained from charged-current processes such as the decays of pions, leptons, and heavy neutrinos. The relevant $W^\pm$ interactions may be written (again following notation from [11]) as

$$\mathcal{L}_{int}^{W\chi^-\chi^0} \equiv -\frac{g_2}{\sqrt{2}} W^{-\mu} \bar{\chi}_a^- \gamma_\mu (P_L \widetilde{B}_{ac}^L + P_R \widetilde{B}_{ac}^R) \chi_c^0 + \text{H.c.},$$

(4.1)

in four-component mass eigenbasis notation. The $\widetilde{B}^{L,R}$ matrices giving the effective coupling strength among the mass eigenstates can be obtained from the diagonalizing matrices of the charged and neutral fermions:

$$\widetilde{B}^L = U_L^\dagger T^L U_0 \qquad \text{and} \qquad \widetilde{B}^R = U_R^\dagger T^R U_0,$$

(4.2)

where

$$T^L = \begin{pmatrix} 0 & \sqrt{2} & 0 & 0 \\ 0 & 0 & 0 & I_{4\times4} \end{pmatrix}$$

and

$$T^R = \begin{pmatrix} 0 & -\sqrt{2} & 0 & 0 \\ 0 & 0 & 1 & 0_{4\times4} \end{pmatrix}.$$

(4.3)

Of particular interest are pion and lepton decays. Here discussion is limited to tree-level decays mediated by a virtual W boson. (Z^0 exchange in lepton decays is negligible for the cases we consider below, the corresponding amplitude being proportional to the product of two μ_i's.) An exhaustive discussion would in principle also require consideration of possible virtual scalar intermediate states. These (together with radiative corrections) would re-introduce trilinear RPV terms; however, as already noted, since supersymmetric scalar particles must be considerably more massive than the gauge bosons, their contributions can be expected to be very small. Partial decay widths for these processes are then given by

$$\Gamma(\pi \to l \bar{\nu}_l) = \frac{G^2 f_\pi^2 |V_{CKM}^{ud}|^2 m_\pi^3}{8\pi} \mathcal{R}_{\pi l} \sum_{c=1}^3 \widetilde{B}_{l\nu_c}^2 P_c^{\pi l}$$

(4.4)

and

$$\Gamma(l' \to l \bar{\nu}_l \nu_{l'}) = \frac{G^2 m_{l'}^5}{192\pi^3} \mathcal{R}_{l'} \sum_{c,d=1}^3 \widetilde{B}_{l'\nu_c}^2 \widetilde{B}_{l\nu_d}^2 P_{cd}^{l'l}, \quad (4.5)$$

where

$$\widetilde{B}_{ac}^2 \equiv |\widetilde{B}_{ac}^L|^2 + |\widetilde{B}_{ac}^R|^2.$$

(4.6)

Standard parameters are the Fermi constant G (see [31] for minor subtleties), the pion decay constant f_π, and V_{CKM}^{ud} = the ud-component of the CKM quark-sector mixing matrix. $\mathcal{R}_{\pi l}$ and $\mathcal{R}_{l'}$ are leading radiative corrections to the processes. The former depends on the pion and charged lepton masses; the latter depends only on the mass of the decaying lepton (See [25,34] for more details.). Finally, the functions $P_c^{\pi l}$ and $P_{cd}^{l'l}$ include the entire phase space factors for the decays as well as parts of the matrix elements—including all dependence on neutrino masses. Explicit formulas from these functions are given in [31]; for use below, $P_c^{\pi l}$ is

$$P_c^{\pi l} = \theta(m_\pi - m_l - m_{\nu_c})[\delta_{l\pi}^2 + \delta_{\nu_c\pi}^2$$
$$- (\delta_{l\pi}^2 - \delta_{\nu_c\pi}^2)^2]\lambda^{1/2}(1, \delta_{l\pi}^2, \delta_{\nu_c\pi}^2);$$

$$\delta_{l\pi} = \frac{m_l}{m_\pi}, \quad \delta_{\nu_c\pi} = \frac{m_{\nu_c}}{m_\pi}. \quad (4.7)$$

As noted previously, Ref. [31] analyzed three-neutrino mixing. The present case differs since mixing of neutrinos with neutralinos (and charged leptons with charginos) is also possible. However, the above formulas remain valid since the new states would be too heavy to contribute to these GeV or sub-GeV decays.

The experimental inputs are the following decay rates:

$$\Gamma(\pi \to e \bar{\nu}_e), \quad \Gamma(\pi \to \mu \bar{\nu}_\mu),$$

$$\Gamma(\mu \to e \bar{\nu}_e \nu_\mu), \quad \Gamma(\tau \to e \bar{\nu}_e \nu_\tau), \quad \Gamma(\tau \to \mu \bar{\nu}_\mu \nu_\tau).$$

Here, by ν_e, ν_μ, ν_τ we mean the states produced alongside the e, μ, τ leptons in the corresponding decays. To eliminate the uncertainty in some of the common factors and thus better isolate the effects of non-SM leptonic masses and mixings, it is preferable to work with ratios [31,11]. For pion decays, we will use

$$R_{\pi\mu}^{\pi e} \equiv \frac{\Gamma(\pi \to e \bar{\nu}_e)}{\Gamma(\pi \to \mu \bar{\nu}_\mu)} = \frac{\mathcal{R}_{\pi e} \sum_i \widetilde{B}_{e\nu_i}^2 P_i^{\pi e}}{\mathcal{R}_{\pi\mu} \sum_i \widetilde{B}_{\mu\nu_i}^2 P_i^{\pi\mu}}. \quad (4.8)$$

For the lepton decays, reduced decay widths are defined by

$$\bar{\Gamma}^{l'l} \equiv \frac{192\pi^3}{G^2 m_{l'}^5} \Gamma(l' \to l \bar{\nu}_l \nu_{l'}) = \mathcal{R}_{l'} \sum_{c,d=1}^3 \widetilde{B}_{l'\nu_c}^2 \widetilde{B}_{l\nu_d}^2 P_{cd}^{l'l},$$

(4.9)

which conveniently allows us to define the ratios:

$$R_{\tau e}^{\mu e} \equiv \frac{\bar{\Gamma}^{\mu e}}{\bar{\Gamma}^{\tau e}} = \frac{\mathcal{R}_\mu \sum_{c,d} \tilde{B}_{\mu \nu_c}^2 \tilde{B}_{e \nu_d}^2 P_{cd}^{\mu e}}{\mathcal{R}_\tau \sum_{c,d} \tilde{B}_{\tau \nu_c}^2 \tilde{B}_{e \nu_d}^2 P_{cd}^{\tau e}} \qquad (4.10)$$

and

$$R_{\tau \mu}^{\tau e} \equiv \frac{\bar{\Gamma}^{\tau e}}{\bar{\Gamma}^{\tau \mu}} = \frac{\sum_{c,d} \tilde{B}_{\tau \nu_c}^2 \tilde{B}_{e \nu_d}^2 P_{cd}^{\tau e}}{\sum_{c,d} \tilde{B}_{\tau \nu_c}^2 \tilde{B}_{\mu \nu_d}^2 P_{cd}^{\tau \mu}}.$$

Barring some miraculous alignment, the physical neutrino mass eigenstates will not be the partners of the charged leptons—the ν_l's above. Nor will they be basis states in the single-VEV parametrization — the ν_i's of Eq. (3.1). The physical eigenstate which acquires a mass at the tree level is denoted by ν_5; we will denote the other two massless degenerate states by ν_{z1} and ν_{z2}. Note that these two light eigenstates are not uniquely defined at tree-level; any linear combination between them is another massless neutrino eigenstate. This indeterminacy will not affect physical results; moreover, the degeneracy will be lifted by radiative corrections.

In the rest of this section, we will discuss implications of experimental constraints on the ratios (4.8) and (4.10). Exact numerical values for rotation matrices U_L, U_R, and U_0 will be used to compute the charged current couplings $\tilde{B}^L$ and $\tilde{B}^R$. However, in order to be able to understand the qualitative features of our numerical results, we find it worthwhile to derive and use approximate analytical expressions for these couplings. To this end, we will use the following approximation. We split the diagonalizing rotation matrices into separate "quasi-MSSM" and "quasi-SM" blocks:

$$U_L = \text{diag}\{R_L, I_{3\times3}\}, \quad U_R = \text{diag}\{R_R, I_{3\times3}\},$$

and

$$U_0 = \text{diag}\{U_4, R_5\},$$

where U_4 diagonalizes the first 4×4 block of $\mathcal{M}_\mathcal{N}$ and R_5 is again the 3×3 CKM-like neutrino mixing matrix. Note that, while this approximation is valid in the small μ_i limit, it is not the same as the approximation used in Sec. II. In that case, all first order terms in the μ_i were kept; here, we keep only those terms of the form μ_i / μ_5. This will be the meaning of the "small μ approximation" in this section.

The SM components of the ν_5 eigenstate are then given by

$$R_5^{i3} = \frac{\mu_i}{\mu_5}, \qquad (4.11)$$

and, by unitarity, the quasi-SM components of the other two eigenstates obey the sum rule

$$|R_5^{i1}|^2 + |R_5^{i2}|^2 = 1 - \left(\frac{\mu_i}{\mu_5}\right)^2. \qquad (4.12)$$

Using Eqs. (4.11) and (4.12) together with the assumption of no right-handed neutrino fields, the quasi-SM sector charged current couplings become

$$\tilde{B}_{l_m \nu_n}^R = 0, \quad \tilde{B}_{l_m \nu_n}^L = R_5^{mn} \Rightarrow \tilde{B}_{l_m \nu_n}^2 = |R_5^{mn}|^2. \qquad (4.13)$$

A. Pion decays

Inserting the small-μ_i approximate expressions from Eqs. (4.11), (4.12), and (4.13) into Eq. (4.8), and disregarding $\tilde{B}_{l_m \chi_n}^2$ contributions involving the more massive quasi-MSSM neutral states (as justified earlier), yields (using $P_{z1}^{\pi l} = P_{z2}^{\pi l}$ for the massless states):

$$R_{\pi \mu}^{\pi e} = \frac{\mathcal{R}_{\pi e}}{\mathcal{R}_{\pi \mu}} \frac{\left[1 - \left(\frac{\mu_1}{\mu_5}\right)^2\right] P_{z1}^{\pi e} + \left(\frac{\mu_1}{\mu_5}\right)^2 P_5^{\pi e}}{\left[1 - \left(\frac{\mu_2}{\mu_5}\right)^2\right] P_{z1}^{\pi \mu} + \left(\frac{\mu_2}{\mu_5}\right)^2 P_5^{\pi \mu}}$$

$$= \mathcal{K}_{SM} \frac{1 + \left(\frac{\mu_1}{\mu_5}\right)^2 \mathcal{P}^{\pi e}}{1 + \left(\frac{\mu_2}{\mu_5}\right)^2 \mathcal{P}^{\pi \mu}}, \qquad (4.14)$$

where

$$\mathcal{K}_{SM} = \frac{\mathcal{R}_{\pi e}}{\mathcal{R}_{\pi \mu}} \frac{P_{z1}^{\pi e}}{P_{z1}^{\pi \mu}} = \frac{\mathcal{R}_{\pi e}}{\mathcal{R}_{\pi \mu}} \left(\frac{m_e}{m_\mu}\right)^2 \left[\frac{m_\pi^2 - m_e^2}{m_\pi^2 - m_\mu^2}\right]^2 = 1.233 \times 10^{-4} \qquad (4.15)$$

is the SM prediction (with $\mathcal{R}_{\pi e}/\mathcal{R}_{\pi \mu} = 0.96103$), and $\mathcal{P}^{\pi l} = P_5^{\pi l}/P_{z1}^{\pi l} - 1$.

The behavior of the $R_{\pi \mu}^{\pi e}$ ratio as a function of μ_5 can be understood by analyzing the dependence of the kinematic functions $P_5^{\pi l}$ on the neutrino mass. Indeed, for a given set of μ_i ratios, the only dependence on μ_5 in $R_{\pi \mu}^{\pi e}$ comes via m_{ν_5} in $P_5^{\pi l}$. Small changes in m_{ν_5} affect $P_5^{\pi e}$ and $P_5^{\pi \mu}$ differently. $P_5^{\pi e}$ increases quite rapidly with increasing m_{ν_5}, as a consequence of matrix element dependence on the masses of decay products in pion decay [for $m_{\mu_5} < 80$ MeV, $P_5^{\pi e} = (m_{\nu_5}/m_\pi)^2$ is a very good approximation]. In contrast, $P_5^{\pi \mu}$ decreases, albeit more slowly, because of the phase space factor. As a result, their ratio $R_{\pi \mu}^{\pi e}$ increases with m_{ν_5}, and this effect is further enhanced the larger μ_1/μ_5 is with respect to μ_2/μ_5.

Looking in more detail at various mass ranges, we find that for $m_{\nu_5} \lesssim 20$ MeV, the kinematic function $P_5^{\pi \mu}$ is nearly the same as the constant $P_{z1}^{\pi \mu}$ ($\mathcal{P}^{\pi \mu} \simeq 0$). In this case, the experimental constraints on the ratio $R_{\pi \mu}^{\pi e}$ can be put in a

simple form in terms of the RPV parameters. Using the 3σ bounds from Table I, we obtain

$$\text{for } m_{\nu_5} \lesssim 20 \text{ MeV:} \quad \frac{\mu_1}{\mu_5} < \sqrt{\frac{1}{137} \frac{m_e}{m_{\nu_5}}}. \quad (4.16)$$

Beyond the threshold value of $m_{\nu_5} = m_\pi - m_\mu = 33.91$ MeV, the π decay into a muon and the massive neutrino can no longer proceed; $P_5^{\pi\mu} = 0$ and the denominator of Eq. (4.14) becomes constant. Then we have the following constraint on the μ_2/μ_5 ratio:

for 34 MeV $< m_{\nu_5} < 139$ MeV:

$$\frac{\mu_2}{\mu_5} < \sqrt{\frac{1}{137}} \quad (\mu_1 = 0). \quad (4.17)$$

Upper limits on the μ_1/μ_5 ratio in this region are given in Fig. 9.

For values of m_{ν_5} of order 100 MeV, the increase in $P_5^{\pi e}$ due to the amplitude contribution are offset by the decrease due to the phase space factor, and $R_{\pi\mu}^{\pi e}$ begins to decrease. At the threshold $m_{\nu_5} = m_\pi - m_e = 139.057$ MeV, the π cannot decay into $e\nu_5$ either. Above this threshold, the $R_{\pi\mu}^{\pi e}$ ratio is constant (in the approximation used here), and the following constraints can be derived:

$$m_{\nu_5} > 139 \text{ MeV:} \begin{cases} \text{for } \mu_2 > \mu_1: & \dfrac{\mu_2^2}{\mu_5^2} - \dfrac{\mu_1^2}{\mu_5^2} < \dfrac{1}{137} \quad \text{(upper experimental bound),} \\[3mm] \text{for } \mu_1 > \mu_2: & \dfrac{\mu_1^2}{\mu_5^2} - \dfrac{\mu_2^2}{\mu_5^2} < \dfrac{1}{82} \quad \text{(lower experimental bound).} \end{cases} \quad (4.18)$$

It must be mentioned that large neutrino masses of $\mathcal{O}(100$ MeV) may be beyond the range of validity of the small-μ_i approximation unless $\tan\beta$ is ''small.'' For $\tan\beta = 2$ and for the MSSM parameters $M_2 = 250$ GeV and $\mu_0 = 100$ GeV, Eq. (3.4) gives $m_{\nu_5} = 149$ MeV when $\mu_5 = 13.9$ GeV, in rough agreement with the see-saw prediction of $\mu_5 = 11.4$ GeV from Eq. (3.3), and thus arguably still within the small μ_5 domain. In addition, radiative corrections to this tree-level calculation may alter the numerical values given above.

Using exact numerical calculations, Fig. 10 shows the dependence of $R_{\pi\mu}^{\pi e}$ on μ_5 for some illustrative ratios among the μ_i's and for the generic MSSM parameter point $M_2 = \mu_0 = 200$ GeV and $\tan\beta = 2,45$. The solid horizontal line denotes a 3σ positive deviation from the experimentally determined central value. The qualitative attributes of the curves agree well with the predictions made above on the basis of the analytic expression (4.14). Note that for large $\tan\beta$, high values of m_{ν_5} are unattainable no matter how large μ_5 is. In this case, values of μ_5 in the hundreds of GeV are allowed.

B. Decays of charged leptons

Equation (4.5) shows that W^*-mediated charged lepton decays are proportional to two $\widetilde{B}_{l_a\nu_c}^2$ factors. This along with the more complicated $P_{cd}^{l'l}$ function (which gives the dependence on the neutrino mass) makes analytic expressions unwieldy, even in the small-μ_i approximation. Hence only results from the exact numerical calculations will be discussed.

$R_{\tau e}^{\mu e}$ of Eqs. (4.10) provides the most interesting constraint, tightening the bound on μ_2/μ_5 in some regions where $R_{\pi\mu}^{\pi e}$ is less effective. A similar conclusion was

reached in [31]. For $\tan\beta = 2$ and μ_1 set to zero, exact numerical results at the generic MSSM point $M_2 = \mu_0 = 200$ GeV show $R_{\tau e}^{\mu e}$ to be more restrictive than $R_{\pi\mu}^{\pi e}$ for $\mu_2/\mu_3 \leq \frac{1}{12}$ and $\frac{1}{4} \leq \mu_2/\mu_3 \leq 1$ (echoing Fig. 6 of [31]). Figure 11a depicts the actual behavior of $R_{\tau e}^{\mu e}$ vs μ_5 at this M_2-μ_0 point for $\tan\beta = 2$ and assorted μ_i ratios. The solid horizontal lines represent 3σ deviations above and below the experimentally-determined central value (which is consistent
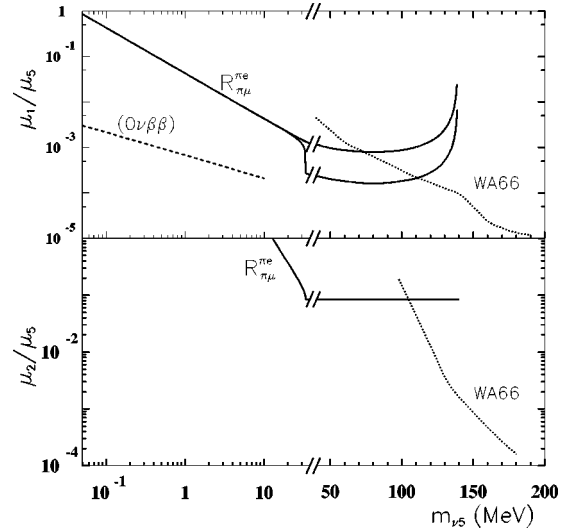

FIG. 9. Constraints on μ_1/μ_5 and μ_2/μ_5 ratios. Solid lines: pion decay [cf. Eq. (4.14)]; in the upper half of the figure, the lower solid line corresponds to $\mu_2/\mu_5 = 1/12$, while the upper line to $\mu_2/\mu_5 = 0$; in the lower half of the figure, the solid line corresponds to $\mu_1/\mu_5 = 0$. Dotted lines: the WA66 experiment (cf. [35]). Dashed line: neutrinoless double beta decay [cf. Eq. (5.2)].
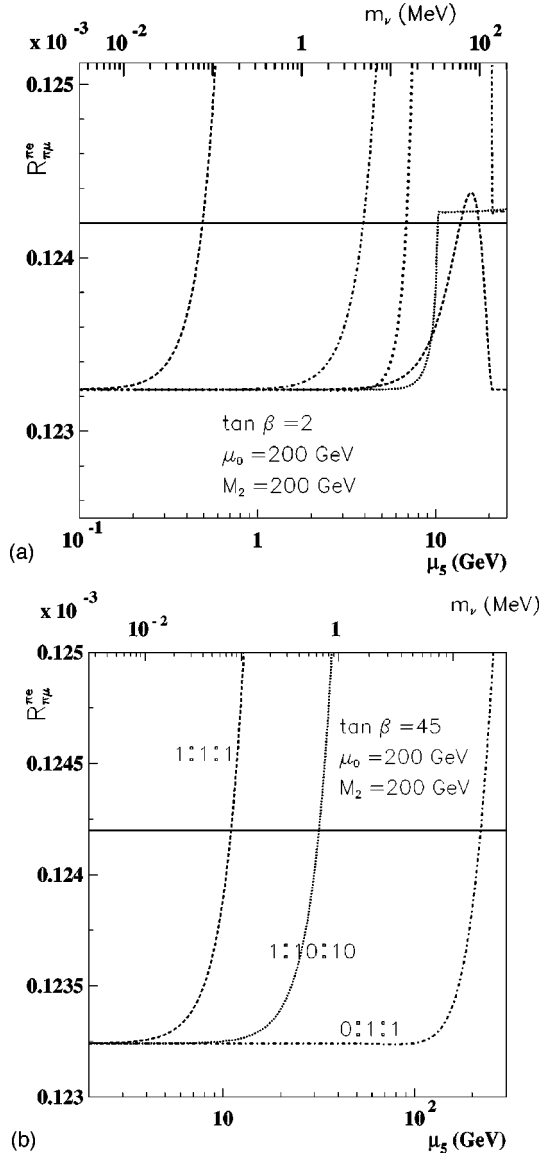
FIG. 10. $R_{\pi\mu}^{\tau e}$ as a function of μ_5 (in GeV) for various μ_i ratios, with $M_2 = \mu_0 = 200$ GeV and (a) $\tan\beta = 2$, (b) $\tan\beta = 45$. In (a) the μ_i ratios are 1:1:1 (long-dashed line); 1:10:110 (dot-dashed line; appears twice in the figure); 0:1:1 (open-spaced dotted line); 0:1:11 (closely-spaced dotted line); 1:0:110 (short-dashed line).

with the SM prediction of 1). For μ_2/μ_3 closer to one ($\frac{1}{5} \lesssim \mu_2/\mu_3 < 1$) and smaller values of μ_5 ($\mu_5 \lesssim 10$ GeV), $R_{\tau e}^{\mu e}$ may dip below the experimentally-allowed band; however, for any $\mu_2/\mu_3 < 1$, $R_{\tau e}^{\mu e}$ eventually goes above the acceptable band as μ_5 is increased. The upper bound on μ_5 only runs from 19.5 GeV down to 17.5 GeV as μ_2/μ_3 is changed from $\frac{1}{12}$ to 0 (values below $\sim \frac{1}{50}$ are indistinguishable from 0). However, the neutrino decay constraints from the WA66 and CHARM experiments described in the next subsection may surpass the constraint from $R_{\tau e}^{\mu e}$ for these somewhat larger μ_5 values.

For high $\tan\beta$, the behavior of $R_{\tau e}^{\mu e}$ vs μ_5 is decidedly different, as seen in Fig. 11b for $\tan\beta = 45$. Here the value of $R_{\tau e}^{\mu e}$ always drops below the experimentally-allowed region as μ_5 is increased irrespective of the $\mu_2:\mu_3$ ratio. The be-
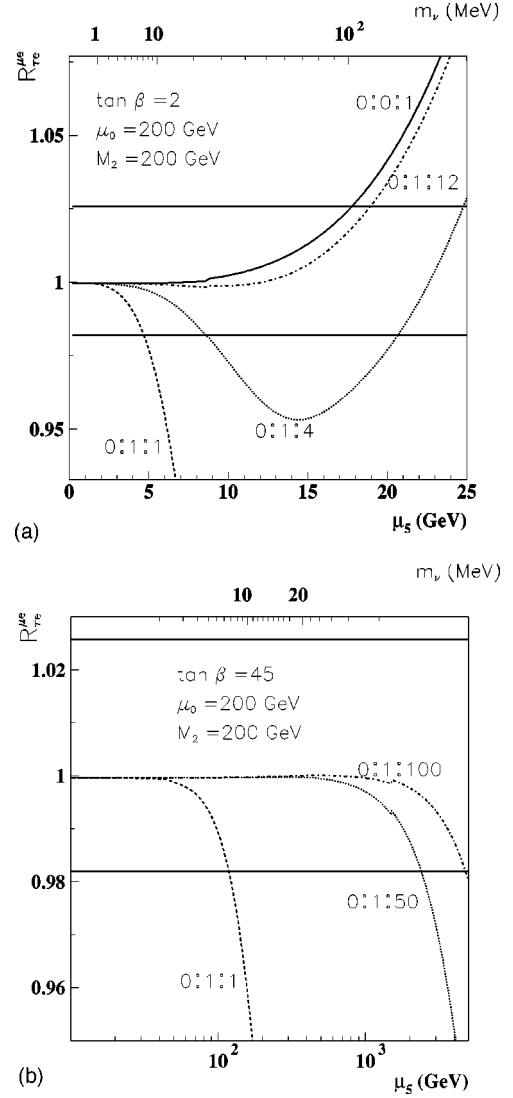

FIG. 11. $R_{\tau\mu}^{\mu e}$ vs μ_5 for assorted μ_i ratios and (a) $\tan\beta = 2$, (b) $\tan\beta = 45$. Horizontal lines denote 3σ deviations from the measured central value as given in [31].

havior is qualitatively reminiscent of that for the $\mu_2/\mu_3 = 1$ curve for $\tan\beta = 2$ even if now μ_2/μ_3 is set to zero. Quantitatively though, the upper limit placed on μ_5 becomes quite large as μ_2/μ_3 drops to zero. This bound is nevertheless still more stringent than that from $R_{\pi\mu}^{\tau e}$ if $\mu_1 \simeq 0$, again irrespective of μ_2/μ_3.

The experimentally-derived values for $\bar\Gamma^{\mu e}$, $\bar\Gamma^{\tau e}$, and $\bar\Gamma^{\tau\mu}$ can also be applied individually without taking ratios. The 3σ bounds on these quantities are also given in Table I. However, these restrictions were always found to be weaker than the constraints from the ratios (in contrast to Ref. [31]).

C. Decays of a massive neutrino

Assuming the decay of the massive neutrino is mediated by a virtual W-boson, the expected decay modes are $\overset{(-)}{\nu}_5 \rightarrow W^{*\pm} l^{\mp}$; $W^{*\pm} \rightarrow l'^{\pm} \overset{(-)}{\nu}_{l'}, (\bar q q' \Rightarrow \pi^{\pm})$.

A crucial experiment restricting this process was performed by the CERN WA66 Collaboration [35] using the

BEBC bubble chamber placed in a neutrino beam resulting from dumping protons on a high density target. The neutrino beam is mainly composed of "prompt" neutrinos from charmed meson decays which can include massive neutrinos up to ~ 1.8 GeV. WA66 is sensitive to massive neutrino decays into electrons, muons, and pions. From the absence of any excess of such events, limits can be placed on mixing of the massive neutrino state with either the ν_e or ν_μ weak-flavor eigenstate. In the small-μ_i approximation, $\nu_l \equiv \nu_i$ and this mixing is simply $|R_5^{mn}|^2 = (\mu_i/\mu_5)^2$. Therefore, the WA66 results can be used to restrict these ratios *if* the small-μ_i approximation is valid; for $m_{\nu_5} \sim \mathcal{O}(100$ MeV$)$, this would demand that $\tan\beta$ is small.

The WA66 results can be summarized as follows (results from CHARM [36] are similar in the parameter regions of interest here). For neutrino mass values of order 100 MeV and above, the mixing parameter μ_1/μ_5 has to be smaller than 10^{-3} ($< 10^{-4}$, for $m_{\nu_5} \sim 149$ MeV). The constraint on μ_2/μ_5 is a little bit weaker: at $m_{\nu_5} = 149$ MeV, $\mu_2/\mu_5 < 10^{-3}$. These limits as a function of m_{ν_5} are presented in Fig. 9. Note that for m_{ν_5} less than $\mathcal{O}(80-100)$ MeV, the constraint on μ_1/μ_5 coming from π decay is stronger than that from WA66, while for $m_{\nu_5} > \mathcal{O}(80-100)$ MeV, the WA66 constraint is stronger. Thus, these two inputs play complementary roles in setting limits on neutrino flavor-state mixings.

The WA66 neutrino decay limits are also used in establishing for the present RPV scenario the 149 MeV absolute upper mass bound on a neutrino which is not a pure ν_τ.[7] As seen above, a neutrino with a mass of 149 MeV is about 99.9% ν_3 which is now extremely well aligned with the τ lepton. In this case the tighter LEP bound of $m_{\nu_\tau} < 18.2$ MeV is applicable; therefore, the upper mass limit on a mixed massive neutrino state is ~ 149 MeV as adopted here.

There are other experiments on neutrino interactions which constrain the mixing among the three generations (for example, the CHARM II experiment [37] on ν_μ-e scattering, and LAMPF [38] on ν_e-e scattering). Some of the resulting constraints are stronger than the WA66 results. However, the interpretation of these data in our current framework (constraints on the RPV parameters μ_i) is straightforward only in the approximation used in this section; otherwise, mixing between the neutrino and neutralino contributions should also be taken into account. For this reason, we have discussed only the WA66 results (for purposes of illustration), leaving a more detailed analysis to a future paper.

V. NEUTRINOLESS DOUBLE-BETA DECAY

Neutrinoless double beta decay ($0\nu\beta\beta$) places very stringent bounds on trilinear RPV parameters, as demonstrated in

---

[7]This result from Ref. [31] is based on a charged current analysis of $R_{\pi\mu}^{\pi e}$, $R_{\tau\mu}^{\tau e}$, $R_{\tau e}^{\mu e}$, $\bar{\Gamma}^{\mu e}$, $\bar{\Gamma}^{\tau e}$, and $\bar{\Gamma}^{\tau\mu}$. As mentioned earlier, Ref. [31] only includes 3-flavor mixing, not possible mixing with gauginos and Higgsinos. It should also be noted that this value is given in [31] as a 1σ bound whereas more conservative 3σ bounds are used throughout the present work.

Ref. [39]. The bilinear μ_i RPV couplings can also mediate $0\nu\beta\beta$; therefore, this process warrants serious consideration here. First, however, features unique to this process must be carefully noted. As with pion decay, this process involves (valence) quarks rather than leptons in the initial state. However, unlike pion decay, for $0\nu\beta\beta$ the decay products are not all colorless. Thus transitions can be mediated by W bosons and a Majorana neutrino with mixing to ν_e *or* by scalars (squarks and/or sleptons) and sfermions (gluinos or neutralinos) [40,39]. Tree-level diagrams involving the former pair can derive the neutrino couplings from the RPV bilinear μ_i's, while those involving the latter pair will be proportional to trilinear RPV couplings. For leptonic decays, possible tree-level trilinear RPV λ coupling dependence due to scalar intermediates was neglected on the grounds that this would be kinematically suppressed since sleptons and Higgs bosons are more massive than the gauge bosons (and the trilinear couplings are expected to also be small). In contrast, with $0\nu\beta\beta$ there are strongly-interacting sparticle intermediates which could perhaps off-set the simple kinematic suppression; thus, trilinear RPV couplings might play a significant role at the tree level for this process. It should be stressed that this is not the case for the previous sections— there the trilinear RPV couplings have *not* been set to zero by hand, they simply do not yield any significant contributions to those processes at the tree level within the single-VEV parametrization augmented by the reasonable assumption of sufficiently heavy scalars. For $0\nu\beta\beta$, in order to concentrate on the bilinear RPV μ_i's, the λ' couplings can be *assumed* to be negligible and/or the squark and gluino masses can be *assumed* to be very large to kill these contributions. Alternatively, to set conservative bounds on the μ_i's it is sufficient to *assume* that there is no destructive interference between the two types of diagrams. A more thorough analysis including the scalar intermediates is underway.

With these caveats, the effective constraint from $0\nu\beta\beta$ becomes [41]

$$m_{\nu_5} |\widetilde{B}_{e\nu_5}^L|^2 < 0.46 \ \text{eV} \quad \text{for } m_{\nu_5} < 10 \ \text{MeV}. \quad (5.1)$$

Applying the small-μ_i approximation, this translates into

$$\frac{\mu_1}{\mu_5} < \sqrt{\frac{0.46}{m_{\nu_5}}} \times 10^{-3} \quad (\text{with } m_{\nu_5} \text{ in MeV}). \quad (5.2)$$

An alternative approximation is to consider only the leading mixing effect between the sole vev-bearing $Y = \frac{1}{2}$ superfield basis state and the other $Y = \frac{1}{2}$ superfield basis states. This yields the approximate expression [cf. Eq. (4.13)]

$$\widetilde{B}_{l_m\nu_5}^L = \frac{\sqrt{\mu_5^2 + \mu_0^2}}{\mu_0} \frac{\mu_i}{\mu_5},$$

and thus

$$|\widetilde{B}_{l_m\nu_{z1}}^L|^2 + |\widetilde{B}_{l_m\nu_{z2}}^L|^2 \simeq 1 - \frac{\mu_i^2(\mu_5^2 + \mu_0^2)}{\mu_5^2\mu_0^2}. \quad (5.3)$$

This approximation should hold even for large values of μ_5. Using this approximation along with Eq. (3.4) for m_{ν_5}, the $0\nu\beta\beta$ constraint is

$$\frac{\mu_1}{\mu_0} < \frac{4.29 \times 10^{-5}}{v \cos\beta} \sqrt{\frac{xM_2}{(xg_2^2 + g_1^2)}}$$

$$\simeq 2.15 \times 10^{-7} \sqrt{(1 + \tan^2\beta)M_2} \qquad (5.4)$$

(with mass parameters in GeV). For the low neutrino mass region in which it is effective, the $0\nu\beta\beta$ constraint on μ_1 (or μ_1/μ_5) is much stronger than that from pion decay, as is seen in Fig. 9. At the generic MSSM parameter point ($M_2 = \mu_0 = 200$ GeV), Eqs. (5.2) and (5.4) require $\mu_1/\mu_5 \lesssim \frac{1}{100}$ for MeV scale neutrino masses and $\mu_1:\mu_0$ of around $1:150\,000$ ($1:15\,000$) for $\tan\beta = 2$ (45)—setting $\mu_1/\mu_5 \sim \frac{1}{100}$ allows μ_5 values of only tenths of a GeV for $\tan\beta = 2$ and a couple GeV for $\tan\beta = 45$.

The limitation from $0\nu\beta\beta$ is only applicable if $m_{\nu_5} < 10$ MeV. Thus the $0\nu\beta\beta$ injunction is turned off if μ_5 is large enough to push m_{ν_5} above this threshold. This means that at any given point in MSSM parameter space, and for $\mu_1 \neq 0$, there will be at least two allowed ranges for $\mu_5:\mu_5 \leq \mu_5^{\beta,max}$ and $\mu_5^{(10)} \leq \mu_5 \leq \mu_5^{max}$, where $\mu_5^{\beta,max}$ is the upper bound from $0\nu\beta\beta$, $\mu_5^{(10)}$ is the μ_5 value at which m_{ν_5} reaches 10 MeV, and μ_5^{max} is the cut-off value due to the strongest constraint aside from $0\nu\beta\beta$ (typically this is from $R_{\pi\mu}^{\pi e}$ for low to moderate $\tan\beta$ values and from $R_{\tau e}^{\mu e}$ for high $\tan\beta$). This of course assumes $\mu_5^{\beta,max} < \mu_5^{(10)} < \mu_5^{max}$ as is almost universally true.

VI. OVERALL COMBINED CONSTRAINTS

Here we pull together all the constraints addressed individually in the preceding sections. These are combined numerically in a comprehensive program to yield a maximum-allowed μ_5 for any given point in MSSM parameter space for a specified $\mu_1:\mu_2:\mu_3$ set. Table I lists all the experimental constraints applied. Note that constraints resulting from the WA66 and CHARM neutrino decay experiments as well as those from neutrinoless double beta decay experiments are not implemented except to rule out potentially admissible large μ_5 regions beyond the first cutoff point for individual constraints (a thorough implementation awaits a more complete analysis including scalar intermediates).

A few details associated with the numerical studies deserve mention. First, (electroweak) gaugino unification is assumed; i.e., $M_1 = xM_2$ with $x = \frac{5}{3}\tan^2\theta_w$. Second, running parameters are evaluated at the scale appropriate to each particular process. Thus for instance Z^0 decays use $\sin^2\theta_w(M_Z)$ while τ decays have $\sin^2\theta_w(m_\tau)$. Specific numerical inputs include (see [12]): $\sin^2\theta_w(M_Z) = 0.2315$, $M_Z = 91.1867$ GeV, and $M_W = 80.4$ GeV.

Figure 12 scans the M_2-μ_0 plane and presents contours of maximum-allowed μ_5 values in GeV. Figures 12a and 12b have $\tan\beta = 2$ while 12c and 12d have $\tan\beta = 45$; $\mu_1:\mu_2:\mu_3 = 0:1:1$ in 12a and 12c whereas $\mu_1:\mu_2:\mu_3$
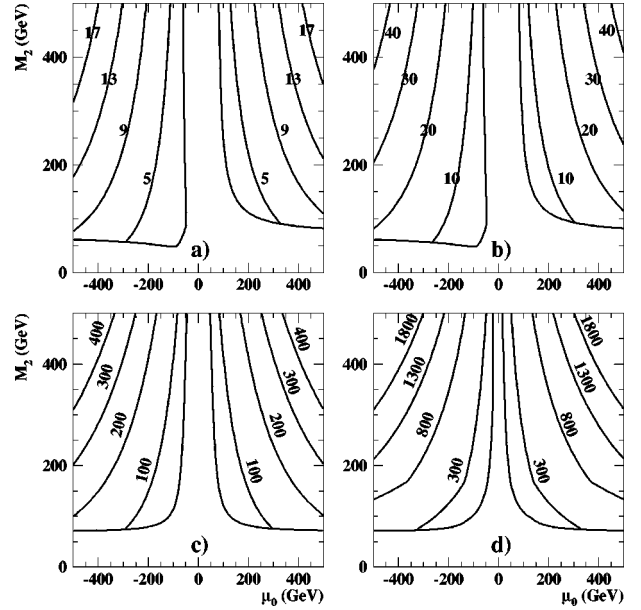

FIG. 12. Maximum allowed values of μ_5 (in GeV) consistent with all the constraints listed in Table I: (a) for $\tan\beta = 2$ and μ_i ratios 0:1:1; (b) for $\tan\beta = 2$ and 0:1:10; (c) for $\tan\beta = 45$ and 0:1:1; (d) for $\tan\beta = 45$ and 0:1:10.

$= 0:1:10$ in 12b and 12d. With $\tan\beta = 2$, the $R_{\tau e}^{\mu e}$ constraint dominates for the 0:1:1 ratio set; but $R_{\pi e}^{\pi\mu}$ is stronger for the 0:1:10 ratio set. The charged current constraints are slightly more restrictive than those from the 149 MeV neutrino mass bound shown in Fig. 7c—the difference is greater when $\mu_1:\mu_2:\mu_3 = 0:1:10$, but the order of magnitude is still the same. If μ_2 is set to zero ($\mu_1:\mu_2:\mu_3 = 0:0:1$), then the 18.2 MeV ν_τ mass bound of Fig. 7a dominates.

Another distinction between Figs. 7 and 12 is in the central region where M_2 or $|\mu_0|$ is small. This region is ruled out in Fig. 12 by limits from processes involving charginos and neutralinos. Such restrictions, embodied in the Table I bounds on the chargino mass, on anomalous "visible" Z^0 decay modes ($Z^0 \to \chi^\pm l^\mp, \chi_c^0\chi_d^0, \chi_d^0\nu; \ d \neq 1$), and on Z^0 full and invisible decay widths, are in general rather conservative, reflecting present intangibles concerning sparticle decays—a more complete study of these is in progress. As discussed in Sec. II E and seen in Fig. 1, μ_i values sufficient to significantly affect the lighter chargino mass are in the high-μ_i realm and thus only depend on μ_5. Results for the combined constraints concur: bounds in the small M_2, small $|\mu_0|$ region are basically independent of the ratios among the μ_i's. One additional point worth noting is that driving up μ_5 to extremely high values will not be able to push up a very small MSSM chargino mass.

Regarding $\tan\beta = 45$: the general pattern of the contour lines is similar to that for the $\tan\beta = 2$ plots; however, admissible μ_5 values are much larger. Upper bounds on μ_5 are relaxed by a factor of $\sim \tan\beta$. The limits in Figs. 12c and 12d are much stronger than those in Fig. 7d which just uses the 149 MeV neutrino mass bound. Both of these changes are due to the dominant charged current constraints ($R_{\tau e}^{\mu e}$ is strongest except for $\mu_1:\mu_2:\mu_3 = 0:1:10$ and $M_2 \lesssim 160$ GeV

in which case $R_{\pi e}^{\pi \mu}$ dominates). As $\mu_2 \to 0$, we again return to the 18.2 MeV m_{ν_τ} limits of Fig. 7b (with the central region again excluded by chargino and neutralino constraints).

VII. CONCLUSIONS AND OUTLOOK

The degree of generality possible within the single-VEV parametrization deserves special notice. With only a trio of inputs (the bilinear μ_i couplings in the superpotential) beyond those of the MSSM[8], the tree-level mass matrices of all color-singlet fermions are completely determined, and a broad range of leptonic phenomenology can be analyzed with a reasonable level of sophistication. Furthermore, the trio can often be collapsed into a single input, μ_5, which carries the full weight of R-parity violation. This is to be contrasted with analyses which either contain a plethora of RPV parameters which preclude a meaningful coverage of the parameter space within the model or arbitrarily pick one or two RPV parameters to be non-zero while the others are all set to zero by hand. As a result, the true freedom within an RPV model will be masked or muddied by a less optimal choice of flavor basis (or by no choice at all).

We have presented tree-level coverage for the variety of electroweak signals summarized in Table I. In the single-VEV parametrization analysis presented here, *the trilinear RPV couplings have not been set to zero*. Rather, they simply do not contribute (at tree level with gauge boson propagators) to the impressive spectrum of leptonic processes studied. In principle, intermediate scalars (sleptons, Higgs bosons) can usher back in the tree-level trilinear dependence; however, such contributions should be suppressed by the larger masses of the scalars relative to the SM intermediate vector bosons, and are nonnegligible only in special regions of phase space. A more in depth look at the scalar sector (along with the related issue of electroweak sparticle decays) is now in progress. An exception to ignoring the scalar intermediates may be necessary with neutrinoless double beta decay due to the presence of strongly-interacting sparticle intermediates. This question is also under study.

Also beyond the present study but slated for future work are loop effects, necessary to describe interesting processes such as $\mu \to e \gamma$. This process may place an additional significant restriction on the μ_i's. Other loop processes will be important in constraining the trilinear RPV couplings. Loops will also lift the degeneracy of the two tree-level massless neutrinos. This extra degree of precision is certainly needed to study the very low-mass neutrinos preferred by several neutrino oscillation experiments. Some models to describe such experiments also suggest that one or more extra light (sterile) neutrinos be added. This could strongly affect the analysis of the charged current constraints presented here, but not the Z^0-mediated neutral current constraints for the charged leptons. Thus, while the charged current constraints are more restrictive, those for neutral current processes are more robust against such possible model extensions.

The single tree-level neutrino mass, m_{ν_5}, depends on the three μ_i only through μ_5. If MeV-scale neutrino masses are allowed, then μ_5 may well be large enough to yield signal rates near, at, or above present experimental bounds for the numerous other processes described herein. Such a neutrino mass is not ruled out by direct or indirect machine (terrestrial) mass bounds. Cosmological constraints favoring light neutrinos may not be applicable; this depends on the decay properties of the massive neutrino and requires more study. An MeV-scale neutrino has been found to be consistent with cosmology in at least one study (which did include fields beyond those in the MSSM) [42].

The results of this analysis reinforce those of [5]: μ_5 values of the same order of magnitude, or even much larger, than M_2 and μ_0 (the standard MSSM inputs) are allowed by the experimental bounds. This is particularly true for high $\tan \beta$ ($\gtrsim 45$), where RPV signals are strongly suppressed. In this case even much tighter bounds on the neutrino mass do not preclude large μ_5 values. This $\tan \beta$ dependence is almost universal among the processes studied. This plus the fact that both the neutrino mass and numerous (though by no means all) approximate expressions for other bounds depend only on μ_5 lead to the interesting question of how much variation is possible among these other processes if μ_5 is fixed.[9] To look at this various possible $\mu_1 : \mu_2 : \mu_3$ combinations were studied using the exact (at the tree level) numerical expressions.[10] A rough hierarchy is seen in the constraints on the individual μ_i's: μ_1 is strongly restricted, μ_2 is less restricted, and μ_3 is still less restricted. This suggests ratio sets of the general form $0:1:x$ ($x \geq 1$). With only two free inputs, this further suggests that, along with a dimensionless ratio, μ_5 is the preferred indicator of RPV effects in leptonic phenomenology.

---

[8]Of course the MSSM already has a fair number of input parameters—M_2, μ_0, and $\tan \beta$ all enter into the mass matrices. This is unchanged and precludes an exhaustive scan of the full beyond-the-SM parameter space.

---

[9]If both μ_5 and neutrino mass are fixed, then restrictions are placed upon the MSSM input parameters. How much $\tan \beta$ dependence and variation is then possible in the remaining processes is currently being investigated.

[10]Naturally, studies that truncate the number of generations cannot preform such analyses and miss very significant and interesting effects.

[1] H.P. Nilles, Phys. Rep. **110**, 1 (1984); H. Haber and G. Kane, *ibid.* **117**, 75 (1985). M. Drees and S.P. Martin, in *Electroweak Symmetry Breaking and New Physics at the TeV Scale*, edited by T.L. Barklow, S. Dawson, H.E. Haber, and J.L. Siegrist (World Scientific, Singapore, 1996), p. 146; H. Baer *et al.*, *ibid.*, p. 216.

[2] *Perspectives on Supersymmetry*, edited by G. Kane (World Scientific, Singapore, 1998).

[3] H. Dreiner, in [2]; G. Bhattacharyya, in ''Tegernsee 1997, Beyond the Desert 1997'' (1997), p. 194; Jose W.F. Valle, hep-ph/9802292, in ''Barcelona 1997, Quantum Effects in the Minimal Supersymmetric Standard Model'' (1998), p. 302.

[4] See, for example, G. Farrar and S. Weinberg, Phys. Rev. D **27**, 2732 (1983); V. Barger and E. Ma, *ibid.* **51**, 1332 (1995); Z. Berezhiani and E. Nardi, Phys. Lett. B **355**, 199 (1995); Phys. Rev. D **45**, 4720 (1992).

[5] M. Bisset, O.C.W. Kong, C. Macesanu, and L.H. Orr, Phys. Lett. B **430**, 274 (1998).

[6] E. Nardi, Phys. Rev. D **55**, 5772 (1997).

[7] C.-H. Chang and T.-F. Feng, hep-ph/9908295.

[8] S. Davidson and J. Ellis, Phys. Lett. B **390**, 210 (1997); Phys. Rev. D **56**, 4182 (1997); S. Davidson, Phys. Lett. B **439**, 63 (1998); J. Ferrandis, Phys. Rev. D **60**, 095012 (1999).

[9] 95% confidence level (C.L.) limits on mixed lepton-flavor Z^0 decays from the OPAL Collaboration, R. Akers *et al.*, Z. Phys. C **67**, 555 (1995); DELPHI Collaboration, P. Abreu *et al.*, *ibid.* **73**, 243 (1997). 90% C.L. limit on $Br(\mu^- \to e^- e^+ e^-)$ from [25]. 90% C.L. limits on flavor-violating τ decay branching ratios from the CLEO Collaboration, D.W. Bliss *et al.*, Phys. Rev. D **57**, 5903 (1998). The 3σ allowable regions for the $U_{br}^{(l_i l_j)}$ and $\Gamma_{Z_{inv}}$ follow from the leptonic partial decay widths found in [12]; 3σ bounds on charged current decay ratios and $\bar{\Gamma}$'s are from 1995 numbers given in [31]. Slightly improved values for $\Gamma(\tau \to e\bar{\nu}_e \nu_\tau)$ and $\Gamma(\tau \to \mu\bar{\nu}_\mu \nu_\tau)$ reported in Pich [30] do not have a significant affect. The 70 GeV chargino bound is very conservative, reflecting uncertainty in detecting the chargino decays.

[10] Here one *caveat* merits noting: we find one set of input m_i consistent with the chosen set of input μ_i's — this does not preclude the possibility that directly solving the 3×3 system of nonlinear equations might also yield another consistent input set of m_i's, perhaps not obtainable by numerical integration from the MSSM $\mu_i = 0$ starting point. For a more extensive discussion, see [13].

[11] M. Nowakowski and A. Pilaftsis, Nucl. Phys. **B461**, 19 (1996).

[12] The LEP Collaborations ALEPH, DELPHI, L3, OPAL, and the LEP Electroweak Working Group and the SLD Heavy Flavour Group, Report No. CERN-PPE-97-154 (1997).

[13] M. Bisset, O.C.W. Kong, C. Macesanu, and L.H. Orr, Proceedings of the 21st Annual MRST Conference: High Energy Physics at the Millenium, Ottawa, Ontario, Canada, 1999, hep-ph/9907359.

[14] J. Bernabéu, J.G. Körner, A. Pilaftsis, and K. Schilcher, Phys. Rev. Lett. **71**, 2695 (1993).

[15] See, for example, W.J. Marciano, in *Precision Tests of the Standard Electroweak Model*, edited by P. Langacker (World Scientific, Singapore, 1995); F. Perrier, *ibid.*

[16] J. Bernabéu and A. Pilaftsis, Phys. Lett. B **351**, 235 (1995).

[17] SLD Collaboration, K. Abe *et al.*, Phys. Rev. Lett. **78**, 2075 (1997); **79**, 805 (1997).

[18] OPAL Collaboration, K. Ackerstaff *et al.*, Eur. Phys. J. C **2**, 213 (1998); ALEPH Collaboration, R. Barate *et al.*, *ibid.* **2**, 417 (1998); M. Bisset, UHM Ph.D. dissertation, UH-511-813-94 (1994); H. Baer *et al.*, FSU-HEP-9504401, hep-ph/9503479.

[19] A.G. Akeroyd, M.A. Díaz, and J.W.F. Valle, Phys. Lett. B **441**, 224 (1998).

[20] A. Joshipura and M. Nowakowski, Phys. Rev. D **51**, 2421 (1995).

[21] See Ref. [6] for an illustration; for additional analyses of neutrino mass see the papers of [22] and E.J. Chun, S.K. Kang, C.W. Kim, and U.W. Lee, Nucl. Phys. **B544**, 89 (1999); V. Bednyakov, A. Faessler, and S. Kovalenko, Phys. Lett. B **442**, 203 (1998); A.S. Joshipura and S.K. Vempati, Phys. Rev. D **60**, 095009 (1999); B. Mukhopadhyaya, S. Roy, and F. Vissani, Phys. Lett. B **443**, 191 (1998).

[22] K. Enqvist, A. Masiero, and A. Riotto, Nucl. Phys. **B373**, 95 (1992); J.C. Romao and J.W.F. Valle, *ibid.* **B381**, 87 (1992); I. Umemura and K. Yamamoto, *ibid.* **B423**, 405 (1994); R. Hempfling, *ibid.* **B478**, 3 (1996); H.P. Nilles and N. Polonsky, *ibid.* **B484**, 33 (1997); B. de Carlos and P. White, Phys. Rev. D **54**, 3427 (1996); A.S. Joshipura, V. Ravindran, and S.K. Vempat, *ibid.* **57**, R5327 (1998); M. Drees, S. Pakvasa, X. Tata, and T. ter Veldhuis, *ibid.* **57**, R5335 (1998); R. Adhikari and G. Omanovic̀, IMSC/98/02/07, hep-ph/9802390.

[23] R. Hempfling, in [22].

[24] ALEPH Collaboration, R. Barate *et al.*, CERN-PPE-97-138 (1997).

[25] Particle Data Group, R.M. Barnett *et al.*, Phys. Rev. D **54**, 1 (1996).

[26] K. Assamagan *et al.*, Phys. Rev. D **53**, 6065 (1996).

[27] H. Baer, V. Barger, D. Karatas, and X. Tata, Phys. Rev. D **36**, 96 (1987).

[28] Super-Kamiokande Collaboration, Y. Fukuda *et al.*, Phys. Lett. B **433**, 9 (1998); **436**, 33 (1998); Phys. Rev. Lett. **81**, 1562 (1998); Super-Kamiokande Collaboration, T. Kajita, Nucl. Phys. B (Proc. Suppl.) **77**, 128 (1999).

[29] In the context of the single-VEV parametrization, see O.C.W. Kong, Mod. Phys. Lett. A **14**, 903 (1999); A. Abada and M. Losada, hep-ph/9908352; K. Cheung and O. C. W. Kong, Phys. Rev. D **61**, 113012 (2000). For other examples, see A. Datta, B. Mukhopadhyaya, and S. Roy, hep-ph/9905549; E. Chun, S. Kang, C. Kim, and U. Lee, Nucl. Phys. **B544**, 89 (1999); J. Romao, M. Diaz, M. Hirrsch, W. Porod, and J. Valle, Phys. Rev. D **61**, 071703 (2000); Y. Grossman and H. Haber, hep-ph/9906310; S. Rakshit, G. Bhattacharyya, and M. Raychaudhuri, Phys. Rev. D **59**, 091701 (1999).

[30] For a recent review, see A. Pich, Nucl. Phys. B (Proc. Suppl.) **55C**, 3 (1997); in ''Cargese 1996, Masses of Fundamental Particles,'' FTUV/97-02, IFIC/97-02, hep-ph/9701263. Also see R.E. Shrock, Phys. Rev. D **24**, 1232 (1981); **24**, 1275 (1981), for a detailed theoretical analysis.

[31] A. Bottino, N. Fornengo, C.W. Kim, and G. Mignola, Phys. Rev. D **53**, 6361 (1996).

[32] R. Cowsik and P. McClelland, Phys. Rev. Lett. **29**, 669 (1972); S. Bludman, Phys. Rev. D **45**, 4720 (1992).

[33] K.S. Babu, T.M. Gould, and I.Z. Rothstein, Phys. Lett. B **321**, 140 (1994); A.D. Dolgov, S. Pastor, and J.W.F. Valle, *ibid.* **383**, 193 (1996); K. Kainulainen, in ''Helsinki 1996, Neutrino Physics and Astrophysics,'' hep-ph/9608215; M. Kawasaki, P. Kernan, H.-S. Kang, R.J. Scherrer, G. Steigman, and T.P. Walker, Nucl. Phys. **B419**, 105 (1994); C. Liu and H. S. Song, *ibid.* **B545**, 183 (1999).

[34] W.J. Marciano and A. Sirlin, Phys. Rev. Lett. **71**, 3629 (1993).

[35] WA66 Collaboration, A.M. Cooper-Sarkar *et al.*, Phys. Lett. **160B**, 207 (1985).

[36] CHARM Collaboration, P.D. Gall, Proc. Neutrino'84 (Dortmund, 1984), p. 193; CHARM Collaboration, F. Bergsma *et al.*, Phys. Lett. **128B**, 361 (1983).

[37] CHARM II Collaboration, P. Vilain *et al.*, Phys. Lett. B **320**, 203 (1994).

[38] LAMPF Collaboration, R.C. Allen *et al.*, Phys. Rev. D **47**, 11 (1993).

[39] M. Hirsch, H.V. Klapdor-Kleingrothaus, and S.G. Kovalenko, Phys. Rev. Lett. **75**, 17 (1995); Phys. Rev. D **53**, 1329 (1996); Phys. Lett. B **372**, 181 (1996); **381**, 488(E) (1996).

[40] R.N. Mohapatra, Phys. Rev. D **34**, 3457 (1986); J.D. Vergados, Phys. Lett. B **184**, 55 (1987); K.S. Babu and R.N. Mohapatra, Phys. Rev. Lett. **75**, 2276 (1995).

[41] L. Baudis *et al.*, Phys. Lett. B **407**, 219 (1997); A. Staudt, K. Muto, and H.V. Klapdor-Kleingrothus, Europhys. Lett. **13**, 31 (1990); K. Muto and H.V. Klapdor, in *Neutrinos, Graduate Texts in Contemporary Physics*, edited by H.V. Klapdor (Springer-Verlag, Berlin, 1988), p. 183.

[42] J.C. Romão and J.W.F. Valle, Nucl. Phys. **B381**, 87 (1992); A.D. Dolgov, S. Paster, J.C. Romão, and J.W.F. Valle, *ibid.* **B496**, 24 (1997); M. Kachelriess, R. Tomas, and J.W.F. Valle, Phys. Rev. D (to be published), hep-ph/0001039.